POLITECNICO DI TORINO

Master of Science in Nanotechnologies for ITCs

Master Thesis

Exploring selective Atomic Layer Deposition of metals for molecular Field-Coupled Nanocomputing prototyping

Supervisors
Prof. Mariagrazia Graziano
Prof. Gianluca Piccinini
Dr. Yuri Ardesi, PhD
Federico Ravera, M.Sc

Candidate
Giorgia Barile

11 April 2024

Abstract

The advancement of nanofabrication techniques is essential for meeting the escalating demands of the semiconductor industry in terms of device miniaturization and performance enhancement. This study focuses on exploring deposition techniques, particularly selective Atomic Layer Deposition (ALD), to propose a feasibility study of molecular Field-Coupled Nanocomputing (molFCN) devices preliminary prototyping. The primary objective is to demonstrate deposition selectivity on substrates with different terminations to enable precise metallic pattern deposition for molFCN fabrication. Specifically, the study examines the potential barriers of half-reactions during ALD of metals (Au, Cu, and Pt) on silicon substrates either stripped or with -H and -OH terminations. The analysis has been carried out through *ab initio* geometry optimizations, Nudge Elastic Band analysis, and Molecular Dynamics simulations utilizing Orca and QuantumATK as computational tools.

The findings reveal variations in potential barriers influenced by the interactions between chosen precursors and the substrate terminations. Specifically, the insights gained into precursor-substrate interactions and the effectiveness of hydrogen passivation revealed that the dangling bonds on the stripped silicon substrate are more reactive than their passivated counterpart, the evidence for this preferential behaviour is evident for Au, less so with Cu and Pt. These findings offer valuable contributions to nanopatterning processes despite the adopted approximations in results due to computational constraints and complexities. Moreover, this analysis provides ground for further investigation potentially addressing the existing gap in the literature on the topic.

Future studies are necessary to evaluate the scalability and sustainability of the proposed techniques to extend the study to larger and more complex samples. Moreover, great emphasis goes to the need for comprehensive force field evaluations to address challenges encountered in molecular dynamics simulations. Additionally, the instability and reactivity of some precursors posed unexpected challenges, therefore further investigation on precursor synthesis stability to improve computational analysis and data reliability.

To all that decided it was worth walking with me

Acknowledgements

I would like to express my deepest gratitude to my supervisors Prof. Mariagrazia Graziano and Prof. Gianluca Piccinini, for their guidance for the duration of this work and especially over my academic years; their boundless competence, prowess and compassion are an endless source of inspiration.

I would also like to thank Yuri Ardesi and Federico Ravera for their admirable expertise, unwavering support and constant feedback, they are the very foundation of this study and without them, this thesis would have never seen the light of day.

I am incredibly grateful for all that these years had to offer, both the good and the bad, all the people I encountered have left an indelible imprint on my life and without every one of them I wouldn't be the person I am today.

I am grateful to the green floor at Collegio Einaudi, my stay there was sadly brief, nonetheless unforgettable, I will always remember the nights in the study room, the early morning rituals and the endless talks, I will always cherish those memories.

Special thanks to all my Giorgias, deep down we are the only ones who can truly understand each other, to Sara and Ed for the time spent together these past years and to Flami for having accompanied me through all the Labs, thank you for all the *aesthetic* you brought to out projects, to Federica, despite being apart, your energy helped me through some of the toughest times, to Federico, faithful companion in misfortune, we are almost there, to Paky and Big, for all the nerdy talks, I would be lost without you, to Antonio, for always wanting to celebrate for and with me, especially when I was too tired to do so, to Stefano, for everything, I probably wouldn't be here without your friendship. I apologize, this thanks came in a bit late for some of you, regardless, thank you for having known me when I could have been everything and for choosing to stay and see what I would become.

Lastly, the most recognition goes to all my family, with particular regard to my Great-grandma Vita, for all the apple slices you left for me, even now that you're gone, to all the Putino family, for all the morning walks to school and all the times you took me in, a particular thanks to Valentina for all the afternoons spent together despite me being the annoying little cousin, you never let me feel left out, to my aunt Giancarla for always lending me your ear and for feeding my stationary addiction and to Nicola for putting up

with us, to my Grandma Carla for all the time you dedicated to me, and to my Grandpa Giovanni for the curiosity you so graciously passed onto me, and to my parents, all abiding source of comfort and support, thank you from the bottom of my heart, this work is as much yours as it is mine, an honourable mention to my Pino, for the much-needed chaos you bring to our lives.

Contents

List of Tables 12

List of Figures 14

List of acronyms and abbreviations 18

1 Introduction 19
1.1 FCN . . . 19
1.1.1 Introduction to molecular Field-Coupled Nanocomputing . . . 19
1.1.2 Technological issues . . . 20
1.2 Introduction to Atomic Layer Deposition (ALD) . . . 22
1.2.1 The ALD process . . . 22
1.2.2 ALD issues . . . 24
1.2.3 ALD precursors . . . 25
1.3 Selective Deposition Techniques . . . 28
1.3.1 Hydrogen Depassivaton Lithography . . . 28

2 Theoretical background 31
2.1 DFT . . . 31
2.1.1 Introduction to the Density Functional Theory . . . 31
2.1.2 DFT conceptualization . . . 31
2.1.3 Khon-Sham method . . . 34
2.2 NEB . . . 38
2.2.1 Introduction to Nudge Elastic Band . . . 38
2.2.2 The basis for NEB simulations . . . 38
2.3 MD . . . 40
2.3.1 Introduction to Molecular Dynamics . . . 40
2.3.2 The MD method . . . 40
2.3.3 The ensambles . . . 42
2.3.4 Force Fields . . . 43

3 Methodology 45
3.1 Geometry Optimization . . . 46
3.2 NEB . . . 49
3.3 MD . . . 49

4 Results 51
4.1 NEB simulations results 51
4.1.1 Gold 52
4.1.2 Copper 60
4.1.3 Platinum 65
4.1.4 Final Data and Considerations 74
4.2 Molecular Dynamics 76
4.2.1 MD QuantumATK method 79

5 Conclusion and future perspectives 85

6 Appendix A 87

Bibliography 91

List of Tables

1.1 Table reporting literature data on film quality, roughness, Temperature and growth rate for different metal ALD processes. 27

4.1 Table reporting the acquired results, extracted from the simulations . . . 75

List of Figures

1.1 molFCN implementation, molecules anchored on a gold nanowire 20
1.2 ALD process: introduction of the first precursor in the chamber and first half-reaction during the first pulse, the chamber is purged by any by-products before proceeding to the second pulse, where the second precursor is introduced. On the right, the final product after 4 deposition cycles . . 22
1.3 ALD temperature window representation 23
1.4 Precursors chosen for the Gold, Copper and Platinum analysis, respectively Me_3AuPMe_3, $Cu(acac)_2$, $Me_2CpPtMe_3$ 26
1.5 STM tungsten tip on an H-passivated silicon substrate, actively removing H atoms (HDL process visualization) 29

2.1 schematic illustration for H-K theorem 33

3.1 Precursors chosen for the Gold, Copper and Platinum analysis 46
3.2 Silicon100 substrates samples with the different terminations (Dangling Bonds, -H, -OH) 46
3.3 Example step1 - initial configuration (in this case Au on H terminated substrate) 47
3.4 Example step2 - final configuration (in this case Au on H terminated substrate) 47

4.1 Reaction pathway, interpolated images 1 to 9 for Au precursor reaction on stripped substrate 52
4.2 Energy pathway of Au precursor reaction on stripped Si100 substrate (step 1 with fixed precursor) 53
4.3 Reaction pathway, interpolated images 1 to 9 for Au precursor on H-passivated substrate (CH4 detachment case) 55
4.4 Energy pathway of Au precursor reaction on H passivated Si100 substrate - CH4 detached from the precursor 56
4.5 Reaction pathway, interpolated images 1 to 9 for Au precursor reaction on H-passivated substrate (Me3P detachment case) 57
4.6 Energy pathway of Au precursor reaction on H passivated Si100 substrate - Me3P detached from the precursor 58

4.7 Energy pathways comparison for all the Au reactions: in yellow, the reaction with the stripped substrate, in blue the reaction with the H-passivated substrate, the case in which the CH_4 is detached from the precursor, in orange, the reaction with the H-passivated substrate, the case in which the Me_3P detached from the precursor 58
4.8 Reaction pathway, interpolated images 1 to 9 for Cu precursor reaction on stripped substrate 60
4.9 Energy pathway of Cu precursor reaction on stripped Si100 substrate (step1 fixed precursor) 61
4.10 Reaction pathway, interpolated images 1 to 9 for Cu precursor reaction on H-passivated substrate 62
4.11 Energy pathway of Cu precursor reaction on H-passivated Si100 substrate 63
4.12 Energy pathways comparison for all the Cu reactions: in blue the reaction with the stripped substrate substrate, in orange, the reaction with the H-passivated substrate 63
4.13 Reaction pathway, interpolated images 1 to 9 for Pt precursor reaction on stripped substrate 65
4.14 Energy pathway of Pt precursor reaction on stripped Si100 substrate (GPC included) 66
4.15 Reaction pathway, interpolated images 1 to 9 for Pt precursor reaction on H-passivated substrate (with counterpoise corrections included) 67
4.16 Energy pathway of Pt precursor reaction on H-passivated Si100 substrate (GPC included) 68
4.17 Reaction pathway, interpolated images 1 to 9 for Pt precursor reaction on H-passivated substrate (counterpoise corrections not included) 69
4.18 Energy pathway of Pt precursor reaction on H-passivated Si100 substrate (GPC not included) 70
4.19 Reaction pathway, interpolated images 1 to 9 for Pt precursor reaction on OH-terminated substrate 71
4.20 Energy pathway of Pt precursor reaction on OH-terminated Si100 substrate 72
4.21 Energy pathways comparison for all the Pt reactions: in blue the reaction with the stripped substrate substrate, in yellow, the reaction with the H-passivated substrate including counterpoise corrections, in orange, the reaction with the H-passivated substrate without the inclusion of counterpoise corrections, in purple the reaction with the OH-terminated substrate 73
4.22 Pt - comparison between GPC inclusion (orange line) and no GPC (blue line) 73
4.23 Passivated Silicon Slab view from the y-axes direction 76
4.24 Passivated surface with Alternating rows of H removed (oovito view on the left, iboView on the right) 77
4.25 Reconstructed and passivated silicon substrate (oovito view on the left, iboView on the right) 77
4.26 Final patterned silicon substrate (oovito view on the left, iboView on the right) 78

4.27 GUIs for the multiple process simulation tool setup 79
4.28 GUI for the potential builder TremoloX 80
4.29 MD simulation results, Copper deposition on top of the Si100 substrate, the simulation was run with 200 events (oovito view above, iboView below) 82
4.30 2D plot of the Sputtering Yield 83

List of acronyms and abbreviations

FCN Field-Coupled Nanocomputing
QCA Quantum Cell Automata
ALD Atomic Layer Deposition
HDL Hydrogen Depassivation Lithography
NEB Nudged Elastic Band
STM Scanning Tunneling Microscope
GPC Growth Per Cycle
DFT Density Functional Theorem
GO Geometry Optimization
NEB Nudge-Elastic Band
MD Molecular Dynamics

Chapter 1

Introduction

1.1 FCN

1.1.1 Introduction to molecular Field-Coupled Nanocomputing

With the increasing demand for faster and more efficient computing systems, Field-Coupled Nanocomputing devices present as a revolutionary computing paradigm as it is proposed as a means to overcome CMOS technology's physical and technological limits such as the limitations imposed by Moore's Law in terms of transistor scaling. FCN stands for Field-Coupled Nanocomputing, which is a computational model that utilizes nanometric molecules to encode and propagate information through local magnetic or electrostatic intermolecular interactions, it poses as the perfect solution as it has potential for digital information processing with low energy dissipation, allows room temperature operation and higher device concentration. By utilizing nanoscale devices and quantum effects, FCN has the potential to revolutionize various fields, including computing, communications, biomedical engineering, etc. FCN has been studied and analyzed from both a low-level analysis of single molecules and a circuit design perspective, to assess its potential and feasibility; momentarily delving into some of the possible applications, devices as field-coupled nanomagnets, can be used for logic gates and magnetically coupled ferromagnetic dots can be engineered for digital information processing (Csaba 2022). However, the application of more relevance to us concerns molecular electrostatic in FCN and QCA, which is a specific implementation of FCN that utilizes quantum dot cells as the building blocks for digital computation. [1]. These devices have attracted significant attention due to their potential for surpassing the limitations of traditional computing systems.

Diving into FCN technological setup, it is mainly structured as follows: A Silicon (Si) trench is etched on the wafer's substrate, a metal nanowire (possibly Gold) is then deposited at the bottom of the trench, as well as Gold electrodes on the sides of the trench for the clocking mechanism. Afterwards, molecules such as Biscerrofene are bonded through thiol groups to the Nanowire in question which acts as a bonding and conducting agent for the molecules.

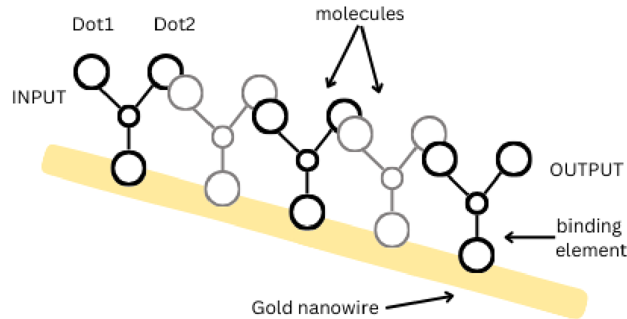

Figure 1.1. molFCN implementation, molecules anchored on a gold nanowire

The information encoding is a quite simple endeavour: the nanometric molecule charge distribution is induced by an external electric field and then propagated through local interactions between the molecules. Therefore, the charge distribution of molecules is used to represent and manipulate information in molecular FCN technology. To encode the two logic states of '0' and '1', two neighbouring oxidized molecules are juxtaposed, creating a QCA (quantum cell automata). The charge distribution and oxidation state of the molecules will repel each other, creating two possible configurations that will be exploited to encode the aforementioned logic states.

1.1.2 Technological issues

For a single MFCN wire, there is a need for a track a few nanometers (even Armstrong) wide, hence, exceptional surface control is imperative both to avoid any verification and synchronization issues due to grain discrepancies and to ensure accurate deposition and etching processes. For more complex patterns, the issues become much greater; most of the already available technological processes cannot guarantee the required level of precision necessary for reliable routing [2], device integration (which involves connecting and organizing the individual components), and surface control. Clocking is also a concern, as it requires an extremely smooth metal deposition and perfect control of the trenches' depth to guarantee coherent synchronization. Nanolithography techniques, such as electron beam lithography and nanoimprint lithography, which can be used to pattern the nanoscale components of these devices are still not viable at large scale and some cannot even reach the needed atomic-level resolution. This brings about the need to address some fabrication challenges such as scalability, reliability, and yield to achieve the full potential of FCN and QCA. Scalability can be defined as the ability of a system to maintain performance and functionality when dealing with large-scale production. Reliability pertains to the stability and functionality of devices with long-term use, even in very different operating conditions. Yield, on the other hand, refers to the percentage of functional devices achieved from the large-scale fabrication process. Deposition methods,

such as physical vapour deposition, chemical vapour deposition, or Atomic Layer Deposition, can be used to deposit the required materials onto the substrates, however, they can prove to be incredibly expensive and present with their set of difficulties which will be examined at a later date.

Ultimately, the thesis's main focus will be a discussion on selective deposition techniques that are relevant to the fabrication of FCN and QCA and how those inspired the analysis that will follow. One such technique is hydrogen depassivation lithography (HDL). This thesis will therefore tackle atomic layer deposition (ALD), which will be the simulated technique using NEB (nudged elastic bands) method.

1.2 Introduction to Atomic Layer Deposition (ALD)

1.2.1 The ALD process

Atomic Layer Deposition (ALD) is a thin film deposition technique that meets the high standard of conformal deposition and atomic layer control exploiting self-limiting surface reactions in order to reach precise thickness and composition control of thin films at the atomic scale.

Most ALD processes are carried out in pulsed mode: The substrate is alternately exposed to precursor gas phases, where the substrate is exposed to the precursors, and purge phases, where the gases are removed from the chamber, this process is repeated until the film reaches the desired thickness. Each precursor gas, when introduced in the chamber, will react with the substrate surface in a self-limiting manner, forming a monolayer of deposited material. This process can be called self-limited since the reaction sites on which the precursor is usually chemisorbed are finite, hence, once the adsorbates have saturated the sites on the surface, the condition for the reaction vacates, preventing any further growth. Therefore, process repetition allows for precise control of film thickness and uniformity. The purge phases in between the precursor phases are necessary to separate the reaction into two half-reactions to prevent any gas phase reactions and avoid substrate contamination during the deposition process.

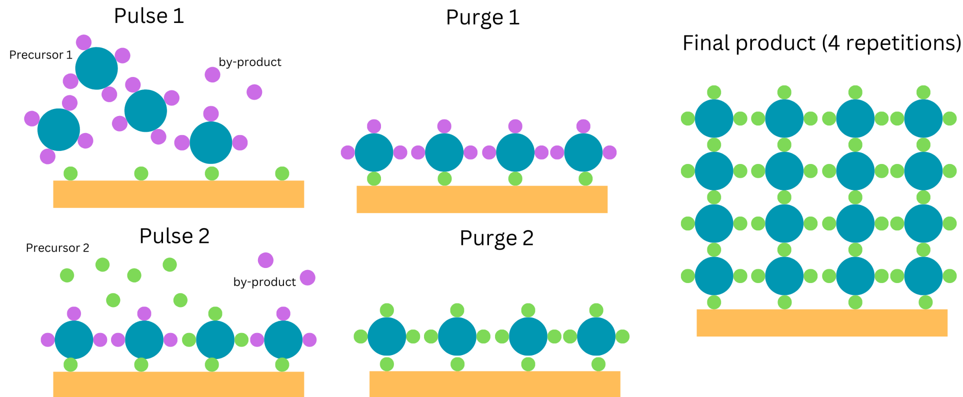

Figure 1.2. ALD process: introduction of the first precursor in the chamber and first half-reaction during the first pulse, the chamber is purged by any by-products before proceeding to the second pulse, where the second precursor is introduced. On the right, the final product after 4 deposition cycles

In Atomic Layer Deposition (ALD), Growth per Cycle (GPC) is an important parameter that determines the linear growth of the desired material and ensures layer-by-layer deposition. Ideally, it should remain constant as it indicates one mono-layer deposited regardless of precursor exposure time. This condition should guarantee linear film growth. However, due to factors such as reactivity, surface site availability, and steric hindrance

(Steric hindrance defines the inability of a molecule to chemisorb on the surface due to the adsorbed molecule dimension which physically inhibits further site occupation), the growth rate can deviate from its ideal value. This leads to two scenarios: substrate inhibition growth, which slows down the growth rate, and substrate enhancement growth, which accelerates it. Moreover, temperature plays a crucial role in determining the GPC. The ALD window 1.3 denotes the temperature range within which self-limiting reactions occur.

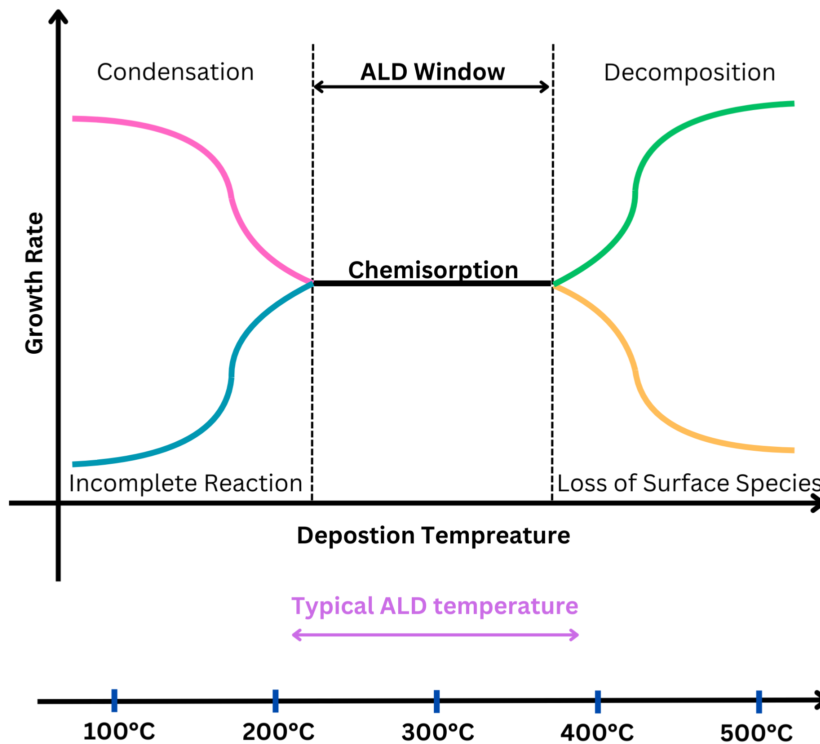

Figure 1.3. ALD temperature window representation

GPC presents as a constant value when inside the ALD window and varies greatly with temperature:

- Lower temperature, lower GPC: low energy doesn't allow for suitable reactions between the precursor and the substrate.
- Lower temperature, higher GPC: Chemisorption is no longer the preferred adsorption mechanism, the precursor is Physisorbed. Physisorption is much weaker

than chemisorption and doesn't guarantee self-limiting reactions, leading to non-conformal and multi-layered films.

- Higher temperature, lower GPC: the chemical reactions on the adsorption sites become unstable due to the higher energy, and the precursor desorbs from the surface.
- Higher temperature, higher GPC: the precursors become themselves unstable, decomposing into other species and introducing contaminant species into the reaction chamber.

Given the process depicted above, one can understand that ALD is an intrinsically slow process: as a result of its layer-by-layer growth and due to its cyclic nature it has an exceptionally slow deposition rate which typically ranges from 0.1Ångstrom to a few Ångstrom per cycle varying with deposition conditions (such as Temperature and Pressure and so on), chosen precursor and material. However this drawback is counteracted by the fact that usually the necessary thicknesses are awfully small, hence the deposition time becomes reasonable despite the slack process, making ALD an incredibly powerful tool and the most prominent deposition technique in the industry.

Moreover, ALD offers several advantages in the fabrication of any type of atomic-scale device. It assures high-quality film deposition with excellent film conformity, even on complex three-dimensional structures, which is one of the most appealing selling factors. The intrinsic self-limiting nature of ALD processes ensures incredibly precise control over film thickness and composition, ideally resulting in uniform and defect-free films. Additionally, ALD allows for the deposition of a wide range of materials, including metals, oxides, and nitrides, offering flexibility in device fabrication.

Researchers can overcome challenges associated with traditional deposition techniques by utilising Atomic Layer Deposition. ALD provides a powerful tool for fabricating nanoscale components with precise control over film properties. In conclusion, the advancements in ALD technology can and will contribute to the development of high-performance FCN and QCA devices.

1.2.2 ALD issues

Despite the many advantages that such advanced technology brings to the table, ALD is renowned for its capabilities in oxide deposition and presents various flaws when switching to metals. Some of the most prominent issues that metal ALD faces are:

- Precursor Selection and Reactivity: The stability of metal precursors is crucial for the repeatability of the process. Some precursors may degrade or decompose over time, affecting the consistency of film growth and some metal precursors may have limited reactivity or may they can be too reactive and decompose in an undesirable manner. Moreover, most metal precursors present as very big molecules and their size alone can prove to be a major nucleation issue.

- Sensitivity Substrate: materials may interact with the ALD precursors, affecting film quality or causing substrate damage.
- Thermal Decomposition: The temperature at which thermal decomposition occurs is a critical parameter in ALD. It needs to be optimized to ensure efficient precursor decomposition without causing undesired side reactions or damaging the substrate [3]. The thermal decomposition of metal precursors can result in byproducts or residuals. The kinetics of the thermal decomposition reaction play a role in determining the growth rate and uniformity of the thin film, hence thermal decomposition can be at fault for both slow growth rate and for poor film conformity and purity.
- Nucleation and Initiation: Some metals exhibit poor nucleation behaviour, leading to non-uniform or incomplete film coverage[4] [5].
- Growth Purity: Cross-contamination between metal precursors or reactions with residual reactants from previous cycles can lead to the incorporation of unwanted elements into the film, affecting its properties. [6]
- Film Stress and Adhesion: film stress can arise from the lattice mismatch between the film and substrate, it can also arise from thermal expansion coefficient differences, or inherent stress during the deposition process. Poor adhesion can lead to film delamination and peeling, jeopardizing the integrity of the entire structure, chemical interactions with metals at the film-substrate interface are more susceptible to weak adhesion [7] [5].
- Film Conformity: Achieving conformal coverage on three-dimensional structures relies on controlling nucleation at various points on the substrate surface. This can be particularly challenging when dealing with complex or high-aspect-ratio structures, especially with such big precursors, nucleation and site saturation can be incredibly challenging.
- Equipment Compatibility: ALD equipment can be complex and expensive. Moreover, not all the already existing equipment can sustain metal ALD, this entails costly modifications or even more costly new machinery.

1.2.3 ALD precursors

As cited in the previous paragraph, one of the crucial features that can determine a successful and controlled deposition is the choice of Precursor. The precursor is a synthesized molecule composed of the species we wish to deposit and some other elements that provide stability to the molecule and that can react with the second precursor or reactant so that the end result is a conformal monolayer of the desired material. Moreover, the choice of precursor also influences other critical factors such as the temperature window necessary for correct operation and determines film properties, for instance, growth rate, roughness and thickness. Our analysis is mainly focused on how to achieve a good metal nanowire deposition, hence, literature research was focused on metal precursors. Most

of the investigated precursors present similar chemical structures or are composed of the same chemical elements (such as Hydrogen, Carbon and Oxygen) hence, only some of the precursors are reported in this dissertation. It is to be noted that for some of these metals, information is quite scarce since the process is very rarely sanctioned and examined. Some of the data collected regarding film properties for different metals can be found in the table 1.1.

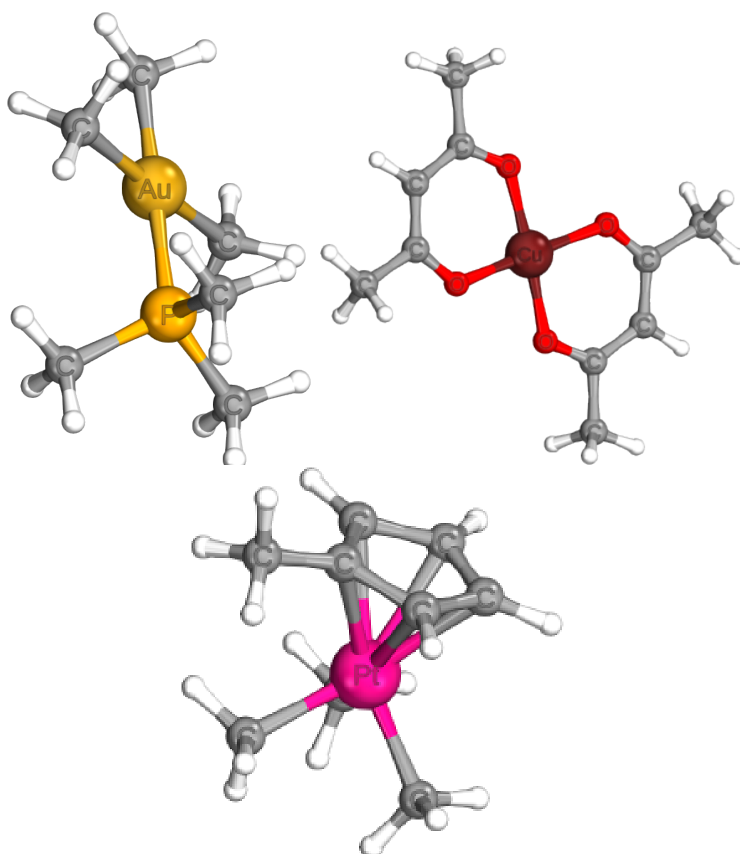

Figure 1.4. Precursors chosen for the Gold, Copper and Platinum analysis, respectively Me_3AuPMe_3, $Cu(acac)_2$, $Me_2CpPtMe_3$

Conclusively, it is necessary to call to attention that this work will mainly be focused on Gold, Copper and Platinum, with particular regard to Gold, as it would be the ideal metal for FCN nanowire production; Copper and Platinum are found to be good substitutes for Gold, and Copper, in particular, makes a valid adhesion layer between the substrate (Silicon) and another metal (such as Gold). The choice in precursors for each of these metals fell respectively on Me_3AuPMe_3, $Cu(acac)_2$, $Me_2CpPtMe_3$ 3.1, mainly because of the presence of exhaustive, although non-complete, literature on the molecules and because are regarded as some of the most stable metal precursors synthesized. They are also volatile, stable and self-limiting, essential qualities for ALD processes, making them the best candidates to proceed with the investigation.

-	Au	Pt	Cu	Ag	Pd
Precursors	Me_3AuPMe_3 [8] [9]	$Me_2CpPtMe_3$[10][11][12]	$Cu(acac)_2$[13] [14]	Ag(hafc) [15]	$Pd(hafc)_2$ [16] [17] [18] [19]
Temperature	120-180°C	275-400°C	250°C	105-250°C	50-80°C
Growth rate	0.09-0.26 nm/cycle	0.47 Å/cycle	0.038 nm/cycle	0.018Å/cycle	0.2Å/cycle
Roughness	-	0.7 nm	10-20 nm	-	4.2-16 nm
Thickness	-	27 nm	200 nm	12 nm	42 nm

Table 1.1. Table reporting literature data on film quality, roughness, Temperature and growth rate for different metal ALD processes.

1.3 Selective Deposition Techniques

The development of selective Deposition techniques will play a crucial part in bettering any type of fabrication process, especially for what concerns nanometric and atomic scale devices, such as FCN.

Such techniques revolve around the possibility of exploiting certain material and chemical properties to make the substrate either more or less susceptible to deposition and etching. Since most of these procedures rely on molecular interactions, they intrinsically possess nanometric resolution. One such technique which has been the origin of this analysis is HDL.

1.3.1 Hydrogen Depassivaton Lithography

Hydrogen depassivation lithography (HDL) can create atomic-scale patterns on a passive surface, which can be transferred into nanoscale structures for applications like quantum computing and etch masks [20]. It represents an incredibly innovative approach to lithographic processes that possess the potential for atomic scale resolution and could prove to be essential for the fabrication of molecular Field coupled Nanocomputing Devices. molFCN are a technological implementation of the computational paradigm Quantum-dot Cell Automata, for which, although for another technological setup than the one of interest, HDL has already been exploited [21]. HDL is based on the selective removal of hydrogen atoms from a surface, using the tip of an STM (Scanning Tunnelling Microscope) which can remove hydrogen atoms from a silicon surface, enabling precise atomic patterning for applications like nanoelectromechanical systems and bio-interfaces [22], for example, atomic precise manufacturing [23] aids the creation of advanced configurations like that of quantum dots, that can be also exploited for another technological implementation for QCA [24]. The substrate is first polished and removed from any contaminants and then, the present dangling bonds are passivated with hydrogen atoms; subsequently, an STM tip is positioned above the passivated surface and a voltage is applied. The applied voltage enables the tip to remove selected hydrogen atoms allowing precise intricate patterning and optimized design implementation. Theoretically, this technique would enable precise patterning which is required for the creation and design of quantum dots and other nanoscale components.

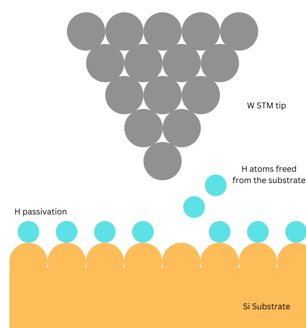

Figure 1.5. STM tungsten tip on an H-passivated silicon substrate, actively removing H atoms (HDL process visualization)

HDL can be exploited in several types of applications: for example, by manipulating individual dangling bonds and erasing them, errors that may occur during the lithography can be corrected [25]; STM-induced desorption and lithographic patterning of Cl-terminated Si(100)-(2x1) surfaces enable the development of halogen-based chemistries for acceptor-based device fabrication[26]; Laser direct oxidation on hydrogen-passivated silicon surfaces allows for the generation of wafer-scale patterns with nanometer resolution, compatible with scanning probe lithography[27]; it can be also exploited to improve the carrier mobility and interface quality of chemical vapour deposited monolayers [28] and it can be a robust approach for fabricating devices with precise control of dopant number, enabling single Phosphorous atoms incorporation at each site of interest using one-dimer patches[29]. As per its general application, HDL can be used to simplify the fabrication process as it reduces the number of processing steps compared to traditional lithography, also, digital fabrication of atomic-resolution patterns on Si surfaces using H depassivation lithography offers high reliability, error checking, and complex system creation.[30] [31]. Ultimately, not only, HDL has been found to be a contender for CMOS consumer electronics production[32], but it has also shown much promise in overcoming traditional lithographic technique challenges like the limited resolution [33] and it could potentially be automated through tools like neural networks[34]; it also offers a method for atomically resolved and controlled nanofabrication with precise control over feature size and density[35]. Furthermore, HDL allows for nanometer-scale metal lines with widths of 10 nm while maintaining resist integrity[36] guaranteeing selective-area growth of metal nanostructures on Si substrates, a very favourable course of action to achieve precise and controlled deposition, moreover, patterned H-resist effectively controls the 3D growth of nanostructures on Si(100) surfaces, limiting precursor adsorption[37] further facilitating deposition purity and accuracy.

Chapter 2

Theoretical background

2.1 DFT

2.1.1 Introduction to the Density Functional Theory

Density Functional Theory (DFT) is regarded as one of the most powerful computational tools in quantum mechanics. It aims to provide a systematic and efficient approach to studying atomic, molecular, or condensed-phase many-body systems.

Developed by Hohenberg, Kohn, and Sham in the late 1960s, DFT has become an indispensable method in theoretical computational chemistry and condensed matter physics. The fundamental premise and advantage DFT proposes lies in the description of the electronic density distribution (density of particles in the ground state of a quantum many-body system), rather than the wave functions of individual electrons; basically, all properties of the system can be considered to be unique **Functionals** of the ground state density.

This approach significantly reduces computational complexity, enabling the study of larger and more complex systems since it doesn't directly solve the many-body Srödinger equation to obtain complete wavefunction, exploiting the concept of electron density, the whole electronic structure can be approximated to a simple Hamiltonian.

The Kohn-Sham equations form the core of DFT, introducing a set of fictitious non-interacting electrons that yield the same electron density as the real system. Despite its approximations, DFT has demonstrated remarkable accuracy in predicting various electronic and structural properties. Following, a brief overview of density functional theory (DFT) will be given. To get a deeper understanding of DFT please refer to [38] and [39].

2.1.2 DFT conceptualization

As mentioned in the brief introduction above, the main objective that led to DFT formulation is the need for an exact theory which can describe any many-body system. A

system constituted by nuclei and electrons is described with its associated many-body Schrödinger equation and Hamiltonian (which is defined as a differential operator describing the total energy of the system in question).

The approximation employed to solve Shrödinger equation and to define the Hamiltonian below is the Born-Oppenheimer approximation, hence the nuclei are considered much heavier than the electrons, and considered in a fixed position.

$$H = -\frac{1}{2}\sum_i \nabla_i^2 + \sum_i V_{ext}(\bar{r_i}) + \frac{1}{2}\sum_{i\neq j} \frac{e}{|\bar{r_i} - \bar{r_j}|}$$

The foundation for DFT mathematical implementation is Hohenberg Kohn theorems (1964).

The first theorem states that for any system of interacting particles in an external potential $V_{ext}(\bar{r})$, the potential $V_{ect}(\bar{r})$ is determined uniquely by the ground state particle density $n_0(\bar{r})$, except for a constant. This entails that the Hamiltonian is fully determined except for a constant energy shift, hence, the many-body wavefunctions for all states (both ground and excited) are determined. Therefore, all proprieties of the system are completely determined given only the ground state density $n_0(\bar{r})$.

This theorem is demonstrated through some hypothesis reduced to the absurd: assuming the existence of two different external potentials which lead to the same ground state density. However, the definition of two external potentials suggests the existence of two different Hamiltonians, with two different ground-state wavefunctions that should however have the same ground-state density. This poses an impossible inequality for non-degenerate states, so, it can be established that there cannot be two different external potentials which give rise to the same non-degenerate state density. The density uniquely determines the external potential (within a constant) and the Hamiltonian is uniquely determined by the ground density (except for a constant); consequently, the wavefunction of any state is determined by solving the Shrödinger equation with its Hamiltonian.

Following, a schematic illustration portraying the Hohenberg-Kohn theorem described above:

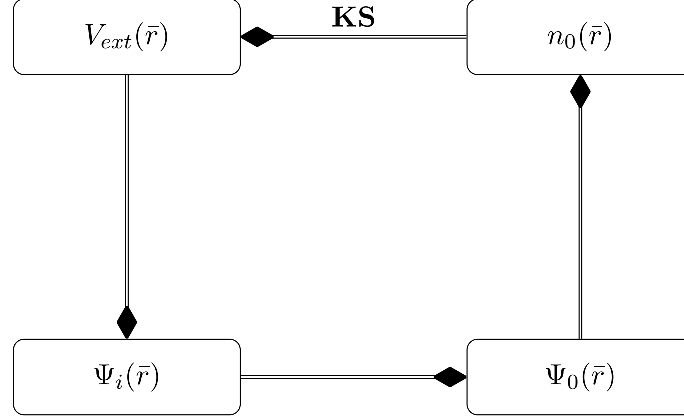

Figure 2.1. schematic illustration for H-K theorem

Despite the appeal of this result, no precise indication has been given to solve the problem, all that was proved is that $n_0(\bar{r})$ uniquely determines $V_{ext}(\bar{r})$, and the core issue persists, we are still left with the problem of solving the original many-body problem of many interacting electrons moving in the presence of an external potential $V_{ext}(\bar{r})$.

Summarizing and providing a somewhat more quantitative description of the issue, $n(\bar{r})$ determines N (number of electrons), the potential V_{ext} and all the properties of the ground state, for example, the kinetic energy $T[n]$, the potential energy $V[n]$ and the total energy $E[n]$.

The dependence on the external potential of the energy functional can be written as:

$$E_{vext} = T[n] + V_{ne}[n] + V_{ee}[n] = \int n(\bar{r})V_{ext}d\bar{r} + T[n] + V_{ee}[n]$$

$$E_{vext} = \int n(\bar{t})V_{ext}\, d\bar{r} \ \ + F_{HK}[n]$$

The term due to el-el interaction may be written as :

$$V_{ee}[n] = J[n] + nonclassicalterms$$

where $J[n]$ is the classical repulsion. The non-classical term is the energy term related to the "exchange-correlation".

$$J[n] = \frac{1}{2} \int d\bar{r}d\bar{r}' \frac{n(\bar{r})n(\bar{r}')}{|\bar{r}-\bar{r}'|}$$

The second theorem providing a foundation to DFT states that a universal functional E[n] defining the energy in terms of the density can be defined, and is valid for any external potential $V_{ext}(\bar{r})$. For any particular $V_{ext}(\bar{r})$, the exact ground state of the system is the global minimum value of this functional, and, the density $n(\bar{r})$ that minimizes the functional is the exact ground state density $n_0(\bar{r})$

For a trial density ñ$(\bar{r})$, such that ñ$(\bar{r}) \geq 0$ and $\int$ñ$(\bar{r})d\bar{r} = N$ (number of electrons):

$$E_0 \leq E[\tilde{n}(\bar{r})]$$

Where E[ñ] is the energy functional of the density in question. This is analogous to the variational principle for wavefunctions[40].

The immediate consequence of the stated theorem is that the energy functional $E[n]$ is sufficient to determine the exact ground state energy and density. In general, the excited states of electrons must be determined by other means.

The proof of this theorem is based on the assumption of the previous: the density determines its very own external potential, Hamiltonian and wavefunction; the latter is treated as a trial function for the problem at hand. Exploiting this second theorem to find the ground state of the trial function and applying the usual constraints requiring that the ground state satisfies the stationary problem, the functional can be written as :

$$E[n] = E_{Ne}[n] + F_{HK}[n]$$

where $E_{Ne}[n]$ is defined as everything that depends on the system and $F_{HK}[n]$ is the Hohenberg-Kohn functional, the part considered universally valid. If the nature and value of the Hohenberg-Kohn functional $F_{HK}[n]$ were known, the equations for the ground state electron density would be known and exact. Moreover, $F_{HK}[n]$ is independent on the external potential $V_{ext}(\bar{r})$; this means that $F_{HK}[n]$ is a **universal functional of the density**.

Once a definite form for $F_{HK}[n]$ is defined, this resolution method can be applied to solve any system. However, accurate calculation and implementation of DFT are far from easy to achieve because the functional $F_{HK}[n]$ is hard to come by in explicit form.

2.1.3 Khon-Sham method

Hohenberg-Kohn theorems provide a theoretical foundation and define tools which would guarantee ease in resolution when faced with a many-body problem, however, they fail to supply a practical way to compute the ground state energy E_0 of a system. The functional $F_{HK}[n]$ can be defined as follows: $F_{HK}[n] = T[n] + J[n] + E_{mol}[n]$, where $T[n]$ is the kinetic energy for the functional, $J[n]$ The classical Coloumb contribution of the

electron-electron interaction and $E_{ncl}[n]$ is the non-classical contribution to the electron-electron interaction energy, of these, only $J[n]$ is known, while the explicit forms of the other two contributions remain undefined and unknown.

To resolve this, Kohn and Sham replaced the original many-body system with an auxiliary independent particle problem introducing a non-interacting reference system built from one electron function, so that the kinetic energy T can be computed with reasonable accuracy. This leads to an exact calculation of the properties of the many-body system using independent-particle methods which makes for remarkably successful approximate formulations.

In more concise terms, Kohn-Sham assumes the ground state density of the original interacting system to be equal to that of the same chosen non-interacting system. Hence, the main assumptions that build this method are:

- The exact ground state density can be represented by the ground state density of an auxiliary system of non-interacting particles
- The auxiliary Hamiltonian is chosen to have the usual kinetic operator and an effective local potential $V_{eff}(\bar{r})$ acting on an electron of spin σ at point $\bar{r}$.

To briefly analytically expand on this, the kinetic energy T can be decomposed into two terms, that of the non-interacting system T_S and the residual part of the true kinetic energy T_C:

$$T[n] = T_S[n] + T_C[n]$$

The Hohenberg-Kohn functional is then defined as:

$$F_{HK}[n] = T_S[n] + T_C[n] + J[n] + E_{ncl}[n] = T_S[n] + J[n] + E_{XC}[n]$$

where $E_{XC}[n]$ is the so-called exchange-correlation energy

$$E_{XC}[n] \equiv T_C[n] + E_{ncl}[n]$$

the exchange-correlation energy as defined above, relates all unknown quantities.

Once defined the variables, to compute the ground state energy E_0 it is necessary to solve the following equations:

$$(-\tfrac{1}{2}\nabla^2 + V_{eff}(\bar{r}))\Phi_i = \epsilon_i\Phi_i \text{ where } i = 1,2,...,N.$$

From which the electron density can be derived:

$$n_0 = \textstyle\sum_i \sum_s |\Phi_i(\bar{r}, s)|^2$$

now the ground state energy E_0 can be easily derived.

The exact form for the exchange-correlation energy E_{XC} intrinsically influences the value for E_0, if known, Kohn-Sham's strategy would lead to the exact energy, hence, the Kohn-Sham approach does not intrinsically introduce any approximations. The approximation only comes into play when the explicit form of the unknown functional is to be derived. In conclusion, DFT allows for access to the ground state energy of a many-body system solving N one-electron Kohn-Sham equations instead of the much more complicated many-body Schrödinger equation. Ideally, there would be no information loss if the exchange-correlation energy is known in its exact form, however, since E_{XC} is unknown, its explicit form is up to guesswork, indeed, introducing an approximation. Kohn-Sham equations can be computationally solved, with well-oiled and relatively straightforward numerical methods, readily implemented in software. Some of the most used computational tools that exploit DFT are VASP, Quantum ESPRESSO or ORCA. A flow chart depicting the computational algorithm some of the listed software adopt is reported below.

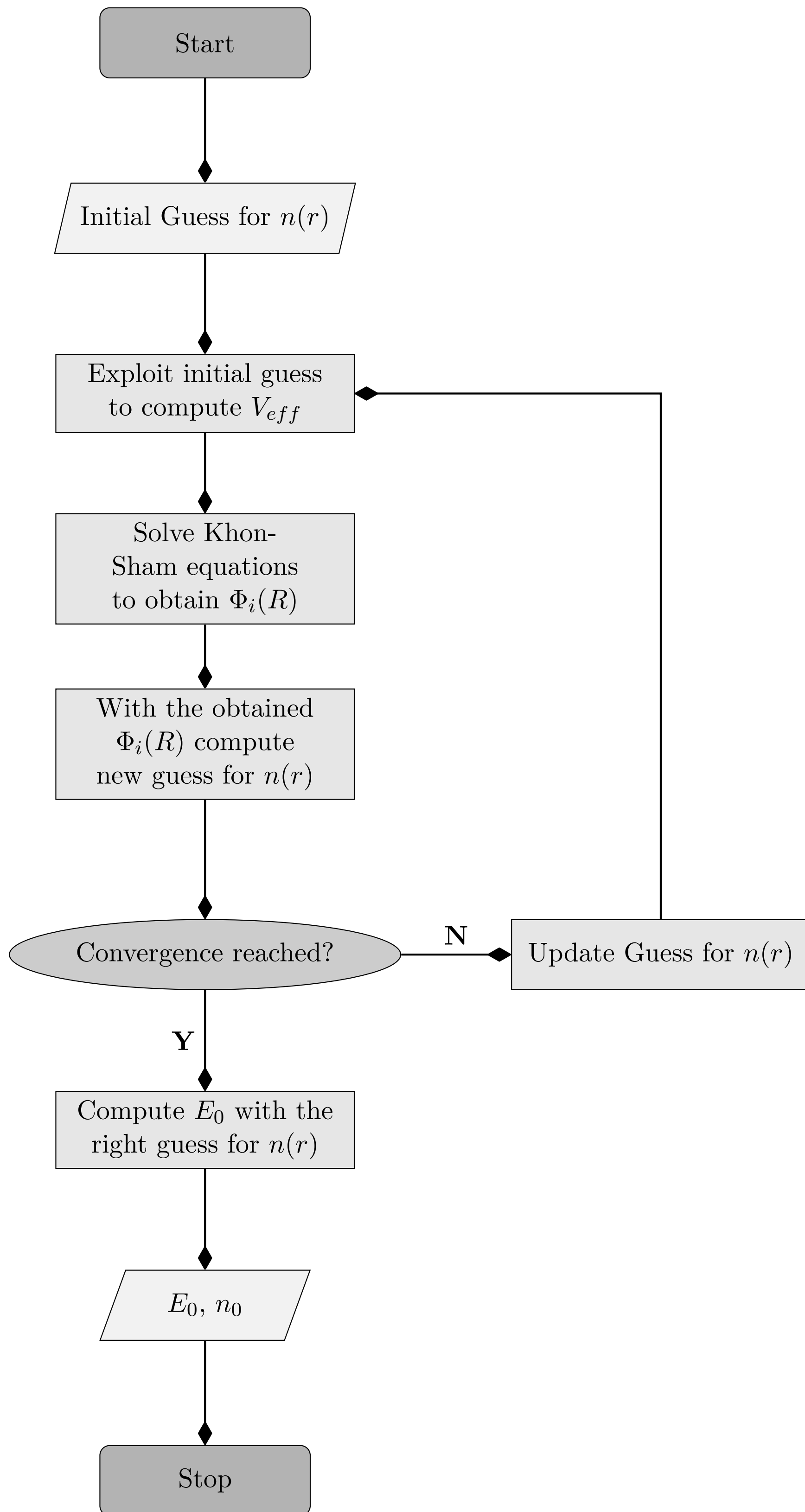
Start
Initial Guess for $n(r)$
Exploit initial guess to compute V_{eff}
Solve Khon-Sham equations to obtain $\Phi_i(R)$
With the obtained $\Phi_i(R)$ compute new guess for $n(r)$
Convergence reached?
N
Update Guess for $n(r)$
Y
Compute E_0 with the right guess for $n(r)$
E_0, n_0
Stop

2.2 NEB

2.2.1 Introduction to Nudge Elastic Band

Nudge Elastic Band (NEB) simulations are a powerful technique mainly exploited in computational materials science and computational chemistry, more generally speaking this technique finds relevance in the field of atomistic simulations. This method is primarily employed to study the mechanisms and pathways of chemical reactions, phase transitions, and other dynamic processes in materials. NEB simulations can be particularly useful for systems with multiple possible reaction pathways, this makes them the perfect tool for ALD reaction analysis as it allows for energy assessment for all possible reaction pathways. Moreover, at its core, the Nudge Elastic Band method aims to find the minimum energy pathway between the two given configurations. The following paragraph will delve into the theory behind Nudge Elastic Band (NEB) simulations in more detail.

2.2.2 The basis for NEB simulations

Interactions between the atoms composing a system can be modelled through interatomic potentials or force fields. These interactions give rise to a collection of energies describing different atomic configurations, creating a so-called *energy landscape*. To better explain, during a chemical reaction, the reactants, intermediates, and products will each correspond to a different configuration composing the *energy landscape*. The energy landscape can be described by a potential energy function $U(\bar{r})$ where $\bar{r}$ represents the coordinates of all atoms in the system. The system is made up of N atoms ($\bar{r}$ is a 3N dimensional vector). To better define the instances that compose the energy landscape, it is imperative to use a *reaction pathway* 4.1.

A Reaction pathway is defined as a series of intermediate configurations that connect the initial and final states of a reaction. In more complex systems, there might be multiple possible reaction pathways, each with its energy barrier.

The reaction pathway is composed of M images, each with its configuration coordinates r_i. These images are generated through a coordinate interpolation between the initial and final states of the system in analysis. The pathway is parameterized by exploiting a reaction coordinate s, where $s = 0$ corresponds to the initial state and $s = 1$ corresponds to the final state.

The NEB method aims to find the **lowest energy pathway** connecting the initial and final state of the given configuration. The pathway is represented as a chain of images, each image corresponds to a configuration along the pathway. Once defined through the interpolation of the system coordinates, the images are connected by imaginary springs (or imaginary spring-like forces), which provide an elastic restoring force that pushes and pulls, the images towards the lowest energy path.

The forces are decomposed into two components:

- The tangential component $F_{t,i}(s)$ that goes along the pathway and drives the images along the reaction coordinate;
- The perpendicular component $F_{p,i}(s)$ which ensures that the images remain evenly spaced along the pathway.

As mentioned above, the images are connected by springs along the reaction pathway, these springs provide an elastic restoring force. Let $r_i(s)$ denote the position of the *i-th* image as a function of the reaction coordinate s. The total potential energy of the system is given by:

$$U((r_i(s)) = \sum_{i=1}^{M} E(r_i(s)) + \sum_{i=1}^{M} \frac{k}{2}||r_{i+1}(s) - r_i(s)||^2$$

where k is the spring constant and $||\cdot||^2$ is the squared Euclidean norm.

The images are nudged iteratively along the pathway to minimize the total potential energy. This is typically done by steepest descent or conjugate gradient methods. The force on each image is calculated as the negative gradient of the potential energy:

$$F_i(s) = -\frac{\partial U}{\partial r_i}$$

To find the transition state of a reaction a variant of the standard NEB method, known as Climbing Image NEB (CI-NEB), is often used. In CI-NEB, one of the images is designated to be the climbing image, and its position is updated using an additional correction term that drives it along the direction of the maximum force. This greatly helps the convergence efficiency of the transition state.

The optimization process continues until the forces on all images are sufficiently small, indicating convergence to a minimum energy pathway.

Overall, NEB simulations provide valuable insights into phase transitions and chemical reactions, allowing behavioural predictions at the atomic level. In conclusion, the NEB algorithm employs coordinates interpolation, elastic band force representation, and numerical iterative optimization to find the minimum energy pathway between two given configurations. This pathway provides valuable information on the kinetics of chemical reactions and phase transitions. More on this can be found at [41].

2.3 MD

2.3.1 Introduction to Molecular Dynamics

Molecular Dynamics (MD) is a numerical method that utilizes classical mechanics to describe the state of a system in terms of space and time. MD solves Newton's equation of motion for a fixed amount of time (time-steps). Time steps are employed to determine the physical interaction among all particles within a given time frame.

MD is a powerful tool that can provide a reliable estimation of the dynamic evolution of a system. It is instrumental when investigating intricate processes in the fields of physics, chemistry, and biophysics. In materials science and engineering, MD is employed as a computational chemistry technique that aids in the study of chemical processes.

By simulating the motion of single atoms in atomic or molecular systems, MD allows for a comprehensive description of the particle system's behaviour. Ab initio approach is based on solving the Schrodinger equation for each particle in the system. While highly accurate, it is also computationally expensive and requires substantial resources. As a result, it is only suitable for a limited number of particles. Nevertheless, despite the difference in accuracy, MD can be used as an exploratory tool to gain initial insights into a system. It also allows for the understanding of systems that are not accessible through experimental techniques. When experimental and simulated results align, it is reasonable to attribute the explanation of the experimental results to the simulation model. However, it is crucial to critically analyze MD results as they may not always be correct, since mainly reliant on classical physics which doesn't account for several microscopic effects.

2.3.2 The MD method

The main objective of an MD simulation is to monitor the movement and the evolution of the atoms in the ensemble in time. A given system with N number of atoms or particles can be described through sets of vectors carrying their respective data for the coordinates and the velocities of each of the particles, during the simulation, the values for position and velocity will be updated for each time instance. The main computational flow will now be quantitatively described and subsequently illustrated by a flow chart which can be found below;

The first computational step is to set up the simulation with the initial positions (and coordinates) and velocities for each particle belonging to the system. Once initialized, the simulation can begin; firstly Newton's laws come into play: the force that each particle exerts on its neighbours is computed:

$$f_{ij} = -\nabla_i V(r_{ij})$$

where $V(r_{ij})$ is the potential energy function and $r_{ij} = ||r_j - r_i||$ is the distance between the two neighbouring particles. Since the force that particle j exerts on particle i has

the same magnitude but in the opposite direction to the force that particle i exerts on particle j (Newton's third law), the total force acting on one particle i is:

$$F_i = \sum_{i \neq j}^{N} f_{ij}$$

Proceeding to the following step, Newtonian mechanics can be exploited:

$$F_i = m_i \bar{r_i} = m_i \frac{d^2 r_i}{dt^2}$$

To assess the time integration of the position and velocity vectors numerical methods are needed. The most accurate, reliable and most exploited numerical method is the Varlet algorithm

$$v_i(t) = \frac{r_i(t+\Delta t) - r_i(t-\Delta t)}{2\delta t}$$

$$r_i(t+\Delta t) = 2r_i(t) - r_i(t-\Delta t) + \frac{F_i(t)}{m_i}(\Delta t)^2$$

Nonetheless, any would suffice, for example, Taylor expansion at the first order:

$$v_i(t+\Delta t) = v_i(t) + \frac{\partial v_i(t)}{\partial t}\Delta t$$

$$r_i(t+\Delta t) = r_i(t) + \frac{\partial r_i(t)}{\partial t}\Delta t$$

However, the simulation would suffer from poor accuracy. The integration leads to the guess for velocity which is then used to compute the kinetic energy and temperature of the system.

As per what concerns the thermodynamics of the system in analysis, all that's left is to account for the total energy of the system:

$$E(t) = U_{tot}(t) + K_{tot}(t)$$

For which the potential component can be computed as the sum of all the potential energies (potential for each pair present in the ensemble):

$$U_{tot}(t) = \frac{1}{2}\sum_{i,j} V(r_{ij})$$

and the Kinteic as the summed-up Kinetic components of the N particles

$$K_{tot}(t) = \sum_{i=1}^{N} V(r_{ij})\frac{1}{2}m_i||v_i(t)||^2$$

Once the Energy of the system is defined, the correlation between the Kinetic component and the temperature is immediate:

$$\frac{2}{3}k_B T = K_{tot}(t)$$

As per the definition of the pressure of the ensemble:

$$P = \frac{N k_B T}{V} + \frac{\sum_{i=1}^{N} F_i \cdot r_i}{3V}$$

Now the position and velocity of every particle of the system have been calculated and updated through time integration and the algorithm can be repeated for the next time-step.

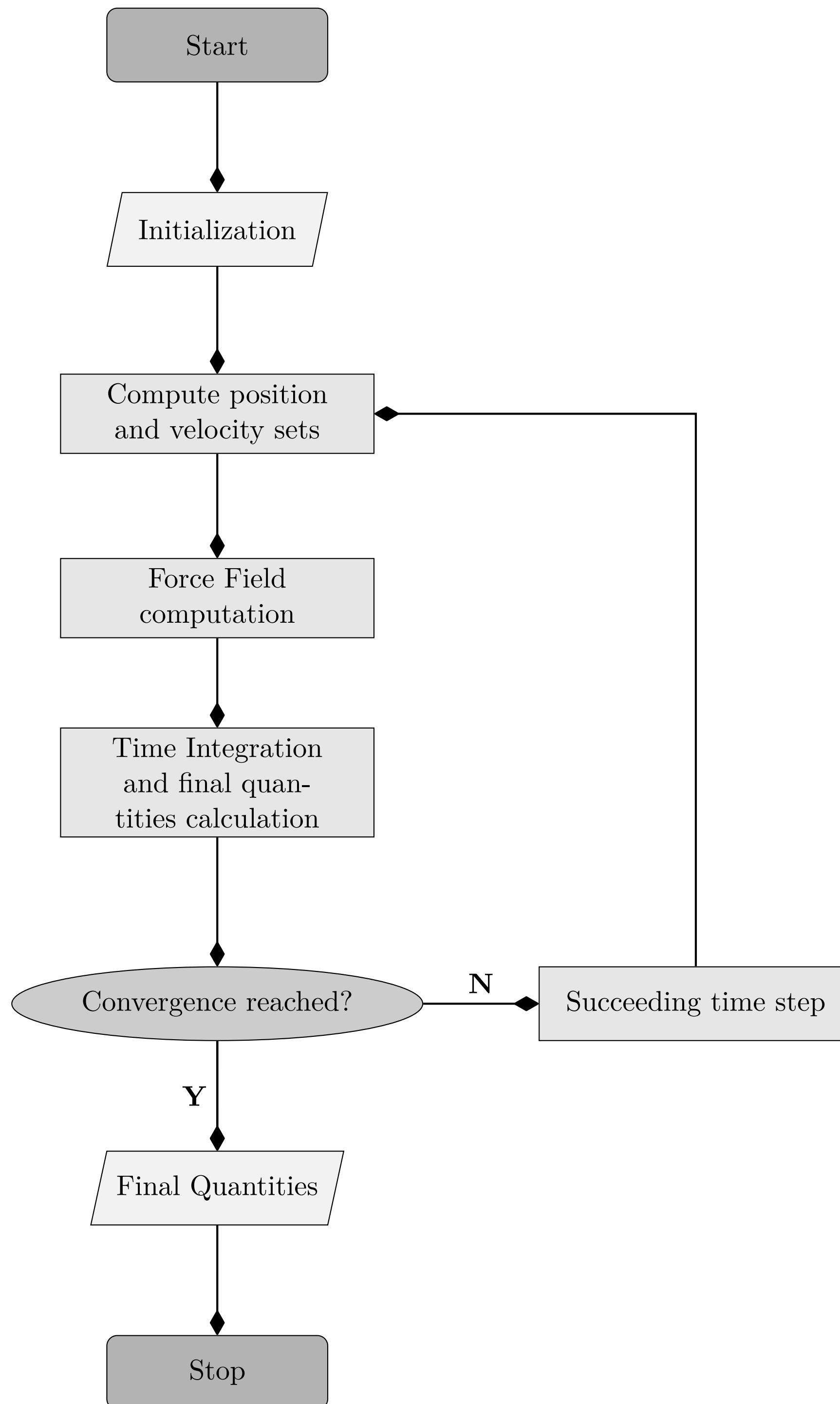

2.3.3 The ensambles

The word *ensemble* has been used quite a bit in the previous paragraph, it refers to the entities that compose the system. It is defined as the N number of particles that

occupy a fixed volume V and has a fixed total energy. The system needs to be completely isolated from the external world and external forces. This system can also be called a micro-canonical ensemble or NVE ensemble, however, in order to have external control over the thermodynamics of the MD simulation, two other ensembles have been defined NVT and NPT:

- **NVT** also called canonical ensemble, sets a fixed temperature by simulating the presence of a heat sink coupled with the system during the simulation. Since the Temperature is externally fixed, the kinetic energy will also be maintained constant. As mentioned, the thermal energy is exchanged through an external thermostat (heat sink), the most used are the Berendsen, the Nosé-Hoover and the Langevin thermostat;
- As per the **NPT**, also called an isothermal-isobaric ensemble, it was previously mentioned, the NVE ensemble is set to have a fixed volume V, hence during the simulation, the pressure will change continuously, to keep the pressure constant, the volume is set to be variable and is adjusted through a barostat, some commonly used are the Berendsen and the Hoover barostat.

A more detailed analysis of the discussed theory can be found [42] [43] [44] [45] [**?**]

2.3.4 Force Fields

Selecting an appropriate potential set for a molecular dynamics simulation depends on the accuracy and efficiency required. MD simulations support various force fields and parameter sets for different materials. Here are a few of the most used potential sets:

- **Universal Force Field (UFF)**; UFF is a general-purpose force field, used for an incredibly wide range of materials, it can be useful for exploratory simulation since it won't make the simulation too computationally expensive, however, this comes at the cost of accuracy since the model lacks quantum mechanical corrections.
- **Reactive Force Fields (ReaxFF)**; ReaxFF is most suitable for any system that includes a chemical reaction since it is very accurate when dealing with bond breaking and bond formation.
- **Tersoff potential**; Tersoff is most often used for silicon-related simulations, it is much less accurate for metals.
- **EAM (Embedded Atom Method)**; EAM is a classical potential, most suited for metallic systems. It is modelled around the electron density of each atom and it is well supported by many software.
- **MEAM (Modified Embedded Atom Method)**; MEAM is an extension of the Embedded Atom Method, it provides an even more accurate description for metallic systems.

to read more about the different models consult the literature and documentation for each potential set to better understand its strengths and limitations [46].

Some factors need to be addressed before making an informed choice:

- **Accuracy**; If the simulation requires quantum mechanical corrections, there might be a need for a more sophisticated potential set such as ReaxFF or even to perform a DFT calculation.
- **Computational Resources**; Computational power poses a hard limit to the simulation, hence, the potential model needs to be in line with the available computational resources.
- **Compatibility**; The chosen model and potential set, need to be compatible with the software employed for the simulation.

The parameters required for a molecular dynamics simulation such as force field parameters or potential set parameters, are typically derived from experimental data or theoretical calculations. These parameters can be obtained through literature and Database research, or computed ex novo through *ab initio* simulations. To avoid computationally expensive *ab initio* simulations, one could check scientific literature and databases for studies on the materials employed in the simulation, since, usually published work is supplemented with force field parameters and potential sets.

Moreover, many force fields, such as ReaxFF, EAM, and Tersoff, come with associated manuals or original papers that provide detailed information on the parameterization process.

Furthermore, some databases specialize in providing materials-related data, including force field parameters, and, some research groups or institutions maintain repositories of potential sets and force field parameters.

Conclusively, some of the softwares employed to perform the MD simulations, for example, QuantumATK, include documentation which carries information on available force fields and potential sets, along with any required parameters. When possible, parameters are often determined through fitting experimental data or quantum mechanical calculations, and the details of this process are typically described in the literature.

Chapter 3

Methodology

As briefly mentioned in the introduction of this work, the investigation aims to provide a quantitative analysis of the selectivity of a passivated substrate in regard to its stripped counterpart. The study is mainly focused on three metal precursors

- Me_3AuPMe_3, chosen ALD precursor for Gold (Au) [8] [9]
- $Cu(acac)_2$, chosen ALD precursor for Copper (Cu) [13] [14]
- $Me_2CpPtMe_3$, chosen ALD precursor for Platinum (Pt) [10][11][12]

and it will simulate their interaction with the surface of

- stripped Si100 (Silicon) substrate (dangling bond - precursor interaction)
- H-passivated Si100 (Silicon) substrate (H - precursor interaction)
- OH-passivated Si100 (Silicon) substrate (OH - precursor interaction)

during a supposed ALD half-reaction process.

The inquiry on the half-reaction is intended to produce an energy pathway which should have a greater energy barrier for the interaction of the precursors with the H-passivated substrate, thus demonstrating a preferential deposition on the stripped Silicon, the OH-terminated substrate was intended to be a control sample, however, was not found to be compliant, this point will be expanded upon in the Results chapter.

The simulation setup is composed of two steps:

- Geometry optimization
- NEB simulation

3.1 Geometry Optimization

In order to perform an accurate and somewhat reliable energy evaluation of the system analyzed, an optimization of the plotted configurations has to be performed.

Firstly, to help with simulation time and computational resources, to be able to evaluate the absorption energy and to guarantee that the structures are in their minimum energy state, the precursors and substrates were optimized separately

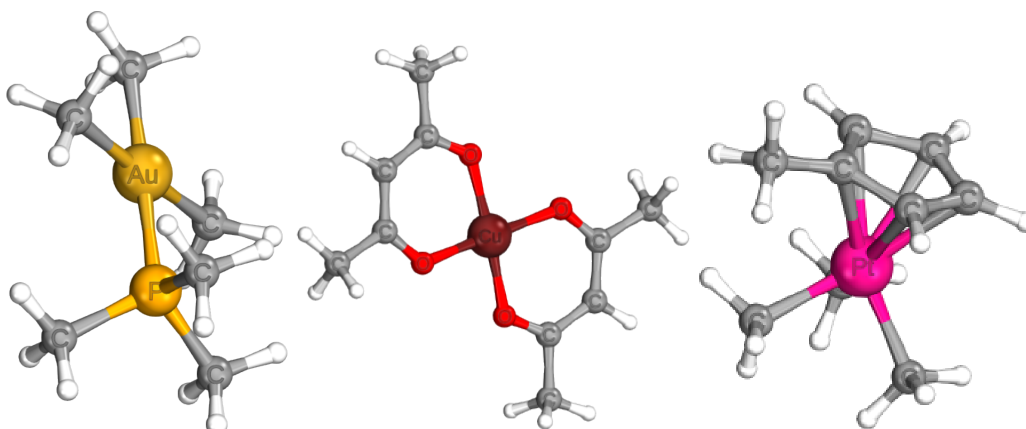

Figure 3.1. Precursors chosen for the Gold, Copper and Platinum analysis

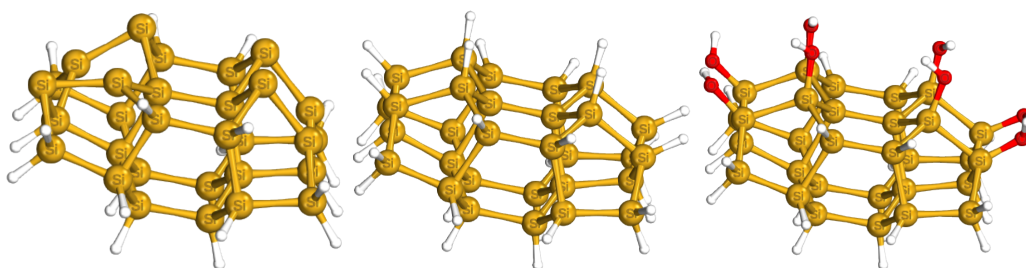

Figure 3.2. Silicon100 substrates samples with the different terminations (Dangling Bonds, -H, -OH)

and then the initial and final molecular structure configurations were set up by combining the precursor and the chosen substrate and optimized

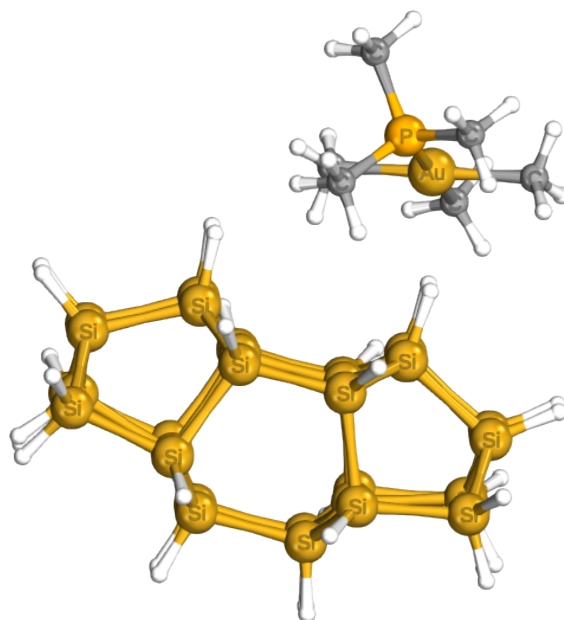

Figure 3.3. Example step1 - initial configuration (in this case Au on H terminated substrate)

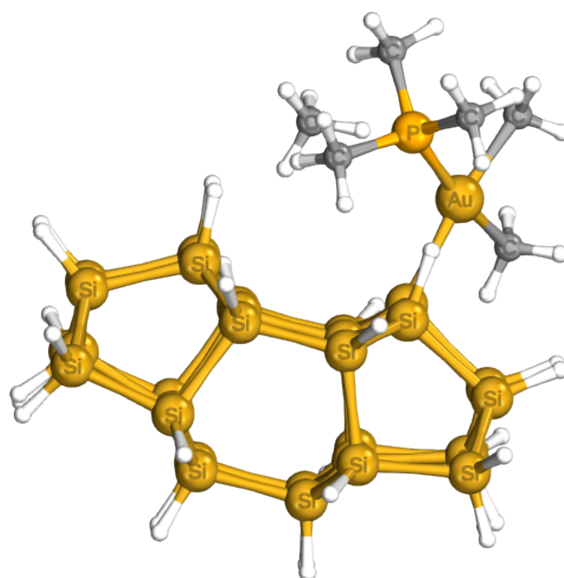

Figure 3.4. Example step2 - final configuration (in this case Au on H terminated substrate)

This process was carried out through the software Avogadro [47]. The molecular coordinates were carefully examined to ensure that they were suitable for ORCA inputs. This process involved checking for correct atom types, atom coordinates and overall geometry.

The Geometry Optimizations (GO) in this study were conducted using the quantum chemistry software ORCA [48] (version 5.0.4). ORCA was chosen due to its capability to perform electronic structure calculations such as geometry optimizations which makes it the optimal choice for exploring molecular structures.

The choice of basis set and quantum chemical method is incredibly significant since their selection can make the difference between accurate electronic structure calculations and implausible results. The chosen basis set was def2-TZVP, were:

- **D**: double-zeta (split into two sets of basis functions: one for core electrons and one for valence electrons)

- **E**: inclusion of polarization functions, they account for the electron cloud's ability to deform in response to the presence of an electron or electron pair and improve the description of electron correlation

- **F2** [49]: specifies that the basis set includes a set of "diffuse" functions, they describe electron density that extends further from the nucleus.

- **TZVP** [50]: "Triple-Zeta Valence Polarized" basis set. This means that the basis set includes three sets of basis functions for valence electrons (one for each level of polarization).

As per what concerns the resolution method, the Perdew-Burke-Ernzerhof(PBE) [51] exchange-correlation functionals have been selected. The Perdew-Burke-Ernzerhof functional, developed by John P. Perdew, Kieron Burke, and Matthias Ernzerhof in 1996, is a widely used Density Functional Theory (DFT) functional in computational chemistry. It is a part of the generalized gradient approximation (GGA) family of functionals. In the PBE functional, the exchange-correlation energy is approximated based on the electron density and its gradients, it also includes non-local exchange effects.

Notably, the simulations also include the dispersion and the counterpoise corrections; The D3 dispersion correction [52] [53] is used to account for Van der Waals interactions, and the counterpoise typically accounts for basis set superposition errors in calculations involving multiple interacting molecules.

The geometry optimization was performed to locate the minimum energy structure of the molecule. The process iteratively adjusts atomic coordinates until SCF Self-Consistent Field (SCF) convergence is achieved. The key parameters, such as the convergence threshold and the maximum number of iterations, were set considering the computational resources available.

3.2 NEB

The Nudged Elastic Band (NEB) [54] method was employed to investigate the reaction pathway and energy changes between the initial and final states of the molecular transformation. This technique provides insights into the mechanisms of chemical reactions by sampling the minimum energy path connecting these states.

As mentioned, NEB calculations require well-defined initial and final states. The structures were produced through Avogadro and based on the desired chemical transformation. These systems were optimized individually using the methodology outlined in GO before being set up in the NEB simulation.

The NEB setup, carefully outlined in the previous chapter, (also performed by exploiting the computational software ORCA, with the same initial setup for the input file as the GO) is based on the interpolation of coordinates, that generate a path of images between the initial and final states. These images, also called beads serve as intermediates of the chemical reaction in analysis. The set of images is then distributed along the pathway, and each bead is subsequently optimized to reach the minimum energy state guaranteeing a smooth transition between adjacent images, an example can be found here 4.1.

Key parameters for the NEB calculation include the number of images (7 in our case) and convergence criteria for each optimization step. The convergence criteria for the NEB calculation were defined to ensure that the optimization process adequately sampled the reaction coordinate. The convergence of the NEB calculation was monitored by tracking the forces on each bead, ensuring that the forces reached a minimum and the band retained its smoothness, indicating a converged reaction pathway. Post-processing for the NEB analysis involved extracting relevant information from the optimized pathway, mainly the reaction coordinate profile, the system structural changes and energy barriers.

3.3 MD

To further our investigation we would also like to perform some Molecular Dynamics simulations in order to check the selectivity of the deposition on a larger scale.

The objective is to:

- Examine a larger substrate, mostly passivated, but patterned.
- Suppose the SPUTTERING process for the deposition
- Verify the efficiency of the "Masked" (Passivated) surface
- Exploiting QuantumATK TremoloX tool to build your own Force Field
- Sputtering yield plot for different angles and energies

Some of these objectives were unfortunately unattainable, nevertheless, a good insight into the used tools was acquired.

Chapter 4

Results

4.1 NEB simulations results

After having laid out the basic methodology employed to carry out the simulations, it's time for a discussion on the obtained data and how it pertains to the findings in the reviewed literature.

Indeed, this section presents the findings obtained from the simulative analysis conducted to address the questions illustrated in detail in the previous chapters, that fueled and motivated this study. Thus, this chapter is mainly focused on data collection, analysis and interpretation and its aim is to provide critical insights into barrier analysis and passivation efficiency, hence, exactly how effective H-masking can be for nano-precise metal Atomic Layer Deposition.

These results are presented both through graphical representation and through numerical data and are displayed to highlight the key patterns and trends discovered during the research process.

This brief introduction serves as a roadmap for navigating the following sections. The findings will be divided into sub-categories, namely by metal deposited and are systematically presented to provide a comprehensive overview of the case study.

As we dive into the results, it is essential to be mindful of the limitations, mainly computational, and challenges faced during the analysis, which will be reported in detail in the following text. Contextualizing the results is important, the findings are completely dependent on the model used for the simulations to better suit the research goal.

In summary, the results section carries the core of the research endeavour, delineating empirical evidence that substantiates the hypotheses posed as a preface for this subject matter.

4.1.1 Gold

Considering that the main purpose that motivates this research is Field-Coupled Nano-computing devices prototyping, and, one of the best materials to fabricate the needed nanowire is Gold, the first simulations that were carried out were in fact centred on this element. Admittedly, Gold is notorious for being one of the most finicky elements to work within the realm of Atomic Layer Deposition, and any fabrication process in general, from deposition to etching is found to be very tedious, mainly because of factors like thermal decomposition, film adhesion and the difficulty in precursor synthesis, hence why it was analyzed first.

The first simulation intended to reproduce the first half-reaction in an ALD process is depicted in figure 4.1.

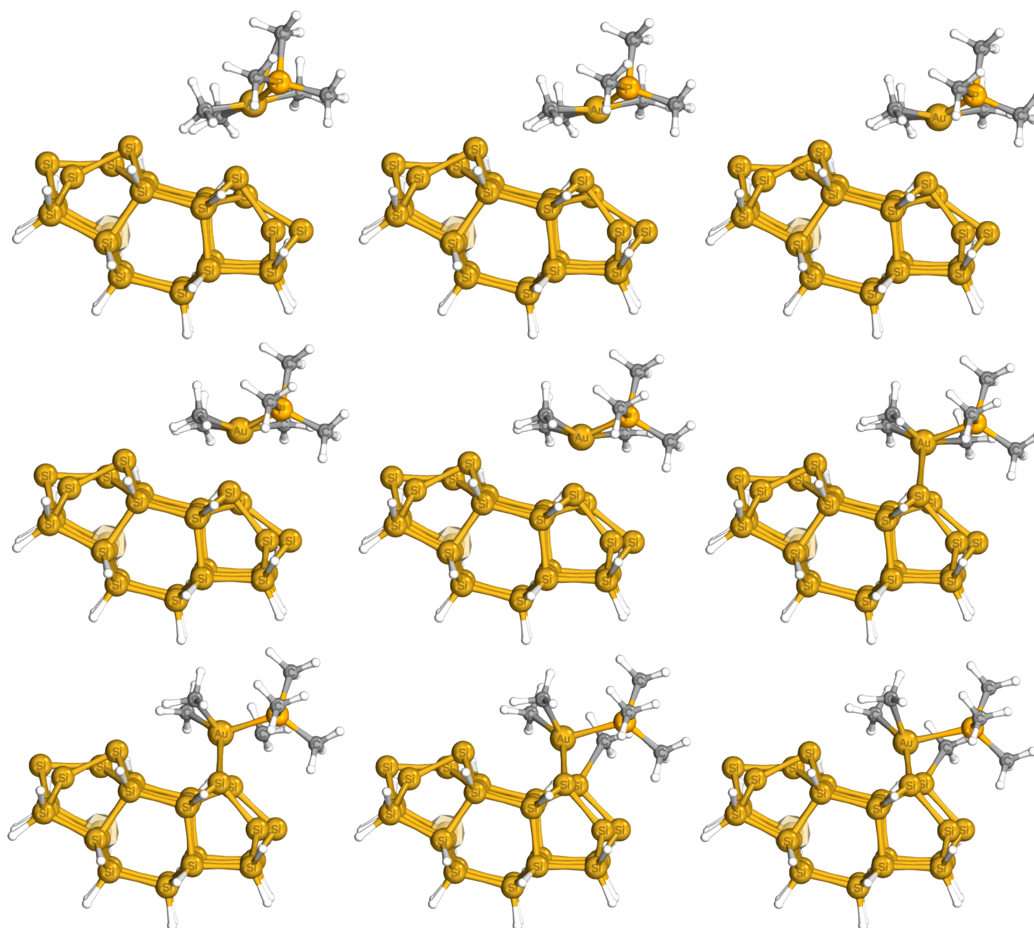

Figure 4.1. Reaction pathway, interpolated images 1 to 9 for Au precursor reaction on stripped substrate

Reading the images from left to right and top to bottom, the first portrays the precursor

(trimethyl(methyl phosphine)gold(I)) hovering on a sample of a Si100 substrate, the surface is completely stripped, hence, the interaction will be between the precursor and the available dangling bonds. The last image represents the final state of the interaction, the precursor is now bonded to the substrate, more precisely, the precursor has been freed from one of its methyl groups which bonded with one of the available silicon dangling bonds, and the recently freed gold electron latches onto another surface silicon atom.

The other images are the result of the NEB coordinate interpolation between the initial and final step and show the most probable pathway the system pursues to reach the final configuration.

For each of these images, or beads, the simulation will provide the total energy of the depicted configuration as output. These data are reported in the figure below 4.2

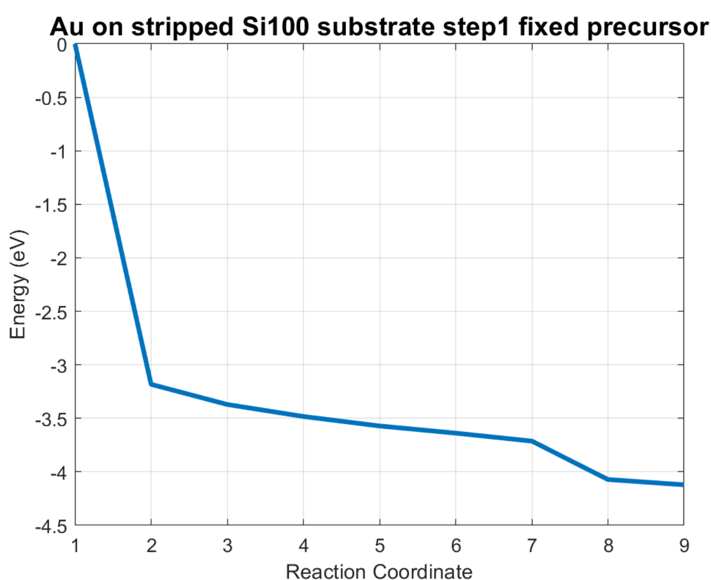

Figure 4.2. Energy pathway of Au precursor reaction on stripped Si100 substrate (step 1 with fixed precursor)

As evident from the plot 4.2, the collection of energy values gathered for each image, results in an energy curve that can be considered as a baseline energy path for the outlined reaction.

More specifically, in this case, the system is found to be highly unstable, the energy falls rapidly, and each of the interpolated images is found to be more energetically inexpensive than the previous, hence, the lack of an energy barrier renders the chemical reaction inevitable.

This result was predictable since the geometry optimization simulation performed on the initial configuration wasn't successful: the precursor bonded with the substrate even if the starting configuration was set up to have a very large gap between the precursor and substrate. In fact, in order to proceed with the NEB analysis, it was necessary to apply further constraints to the structure: the constraints were extended to include the precursor, not only the "bulk" bit of the substrate, with the pretence that during the reaction in question, in a specific instance in time, the structure would have to assume that specific configuration. The purpose of fixing in space the precursor was to "*freeze*" that frame and exploit it as the starting point of the NEB simulation.

Indeed, the NEB simulation was exceptionally insightful, since it provided a graphical explanation (4.2) to the seemingly inexplicable reaction happening during the Geometry Optimization. To put it into better words, there didn't exist a configuration that minimized the total energy of the system where the precursor wasn't bonded to the surface, the evidence of this result can be found in the lack of **energy barrier** in 4.2.

The simulation can be considered successful overall, however, some arising issues are notable:

- The simulation **converged**, still, the Climbing Image (CI) never activated, the simulation had to *approximate to a Unit tangent to the TS (Transition State) mode at the saddle point*, hence, *No barrier was found.* This caused the simulation to be abruptly terminated, yet the output data was deemed solid.
- The inclusion of Counterpoise Corrections [55] caused the *element Au to be treated as Cu*, because of contrasting basis set inclusions in ORCA *Different basis set in ORCA and otoolgcp.* All this was necessary to avoid excessive approximations or errors due to overlapping basis sets.

Due to the underlined issues and the complexity of the configuration, several attempts were made before achieving reasonable results, it was indeed quite difficult to overcome some computational limitations, especially considering the length (time-wise) and the convergence issues encountered.

The following step is to pass onto the analysis of the structure with the passivated substrate; the reaction pathway can go one of two ways, either CH3 detaches from the precursor, bonds with an H atom from the substrate surface and then the freshly created dangling bond reacts with the Au 4.3, or the precursor splits in half, the P-Au bond breaks and trimethyl-phosphate bonds with the Hydrogen that detached from the substrate and the trimethyl-gold reacts with the newly formed dangling bond 4.5.

The initial and final configurations for the first case are depicted in figure 4.3, respectively the upper left and bottom right images.

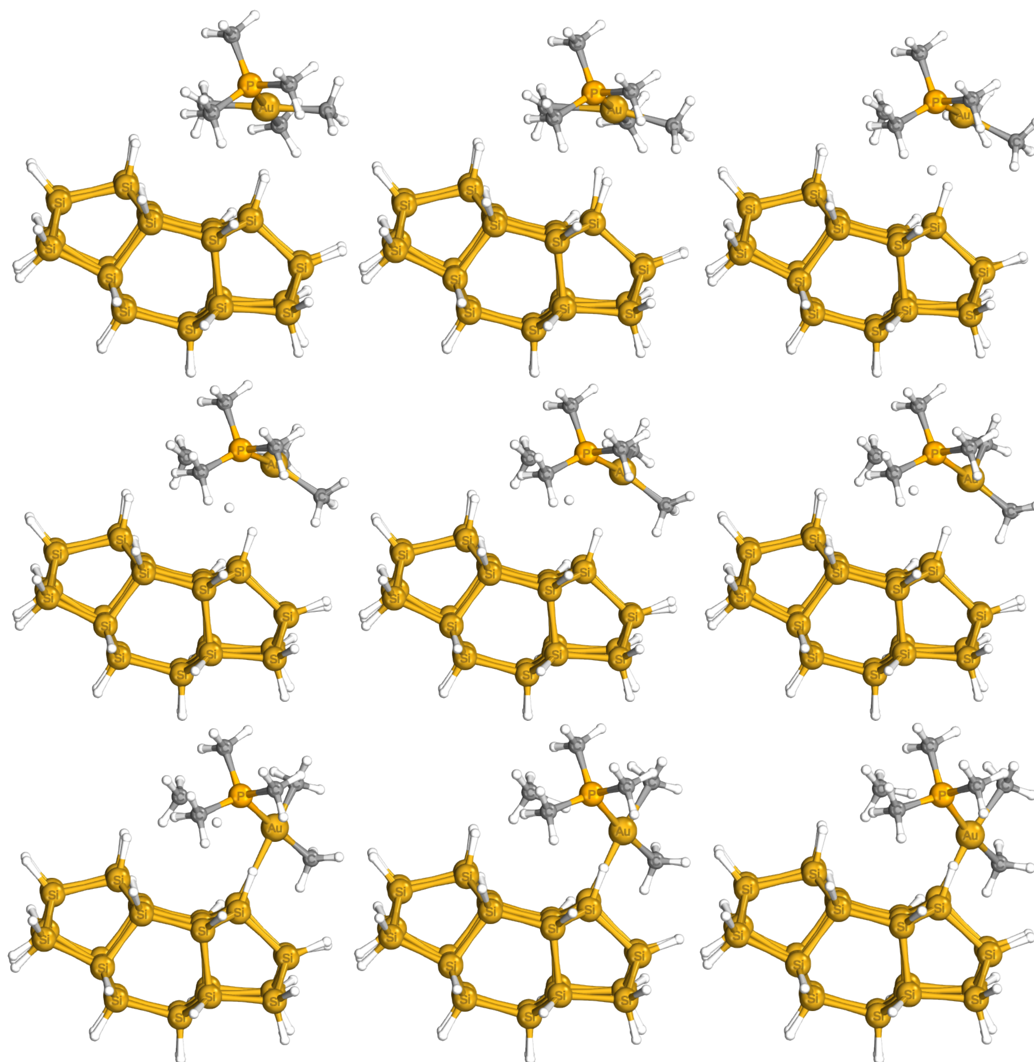

Figure 4.3. Reaction pathway, interpolated images 1 to 9 for Au precursor on H-passivated substrate (CH4 detachment case)

The energy pathway for this configuration is shown in the figure below 4.4

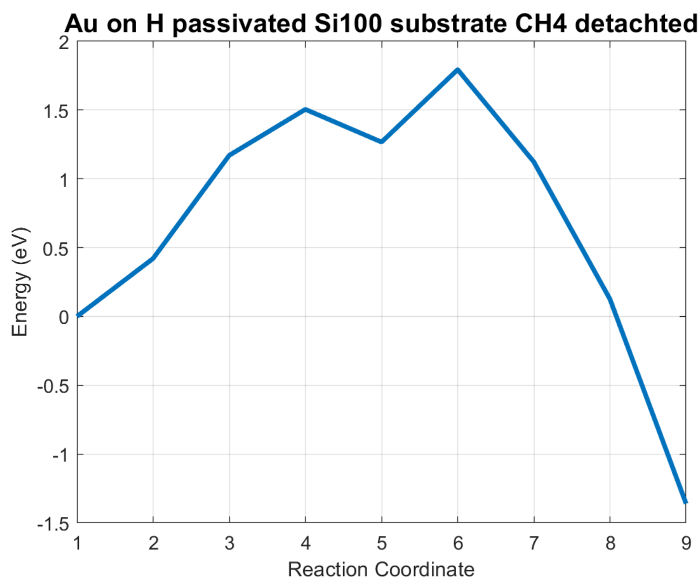

Figure 4.4. Energy pathway of Au precursor reaction on H passivated Si100 substrate - CH4 detached from the precursor

The simulation reached convergence, admittedly after a few failed trials, however, not many issues were encountered, this attests to the stability of this configuration, further underlining the dangling bonds as cause for the issues in convergence in the previous system.

The barrier found, considerably higher than before, further proves the selectivity and the efficiency of the passivation layer.

Two local maxima, one in image 4 and the higher one in energy at image 6 are visible in the plot 4.4, and a considerable decrease in energy for the final step is observed. This indicates that the final configuration is far more energetically stable than the initial, however in order to reach the more stable confirmation, it is necessary to overcome the barrier, in more simple words, it is necessary to provide energy to the system.

Now, for the second configuration, the pathway images can be visualized in 4.5:

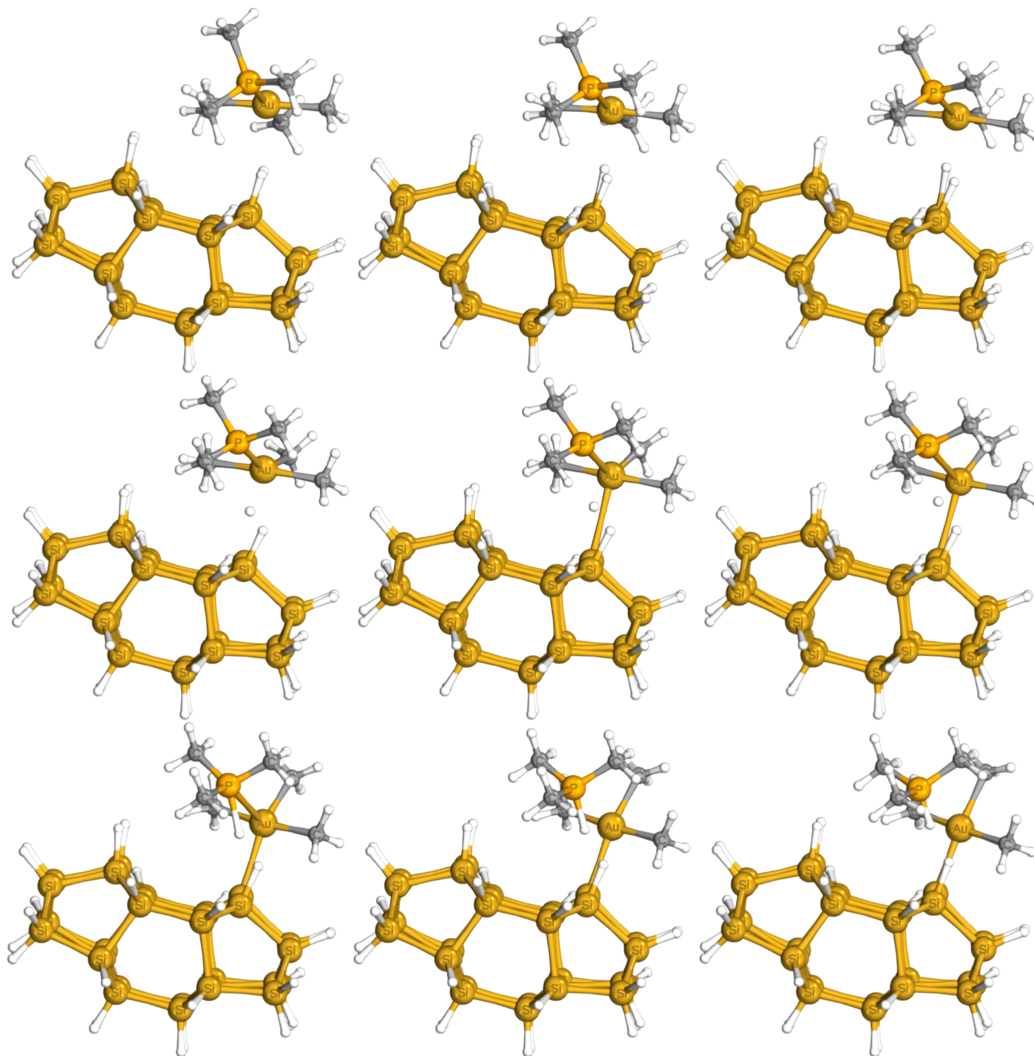

Figure 4.5. Reaction pathway, interpolated images 1 to 9 for Au precursor reaction on H-passivated substrate (Me3P detachment case)

Here one maximum, again in image 6, the final configuration (image 9) has higher energy than the first (image 1), hence, this pathway 4.6 will be less probable than the previous. As per what concerns about the convergence of this simulation setup, the NEB section reached convergence, however the subsequent SFC optimization reached the maximum number of iterations without getting to completion.

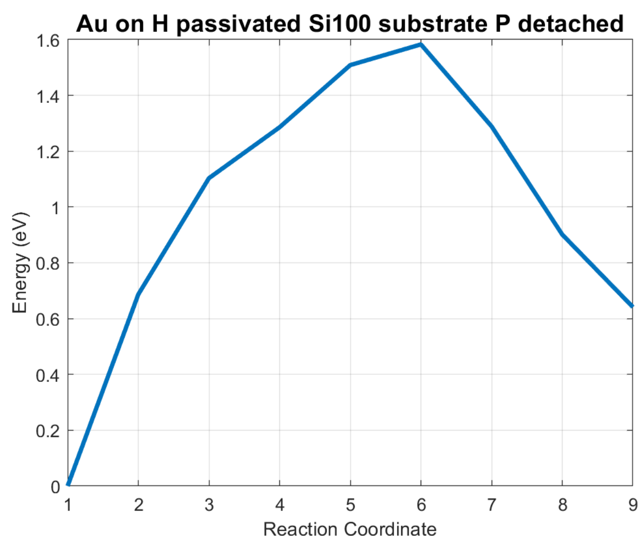

Figure 4.6. Energy pathway of Au precursor reaction on H passivated Si100 substrate - Me3P detached from the precursor

To gain a better insight and understanding of the main differences between the energy pathways, a comprehensive plot has been made 4.7. The difference in the potential barriers between the passivated and stripped configurations is glaring. Also, the difference in final energies is evident, and, as mentioned before, it gives us an esteem of the preferred path of the chemical reaction.

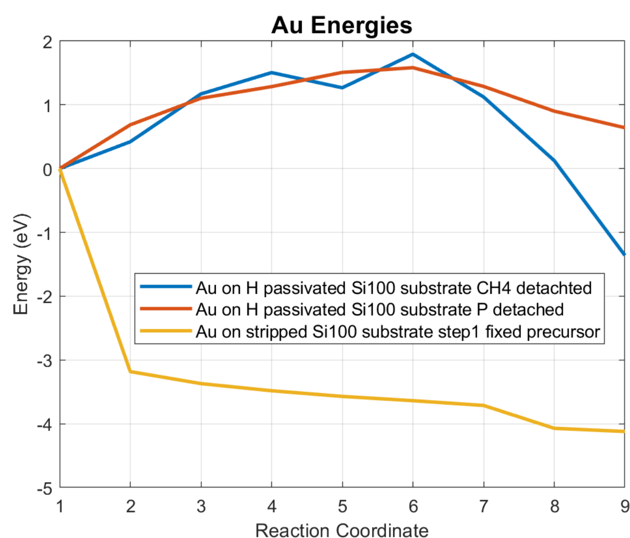

Figure 4.7. Energy pathways comparison for all the Au reactions: in yellow, the reaction with the stripped substrate, in blue the reaction with the H-passivated substrate, the case in which the CH_4 is detached from the precursor, in orange, the reaction with the H-passivated substrate, the case in which the Me_3P detached from the precursor

To sum up the considerations that have been made, Gold remains one of the trickiest metals to work with in terms of deposition, even in the simulative realm, however, despite its difficulties and limitations, passivation effectiveness was indeed demonstrated. A more detailed and quantitative data collection which further settles this point can be found at the end of this section 4.1.

4.1.2 Copper

The same process was employed for copper, in this case, Copper(II) Acetylacetonate was the chosen precursor.

The technological setup is comparable to the previous, an overview of the structure is in figure 4.8.

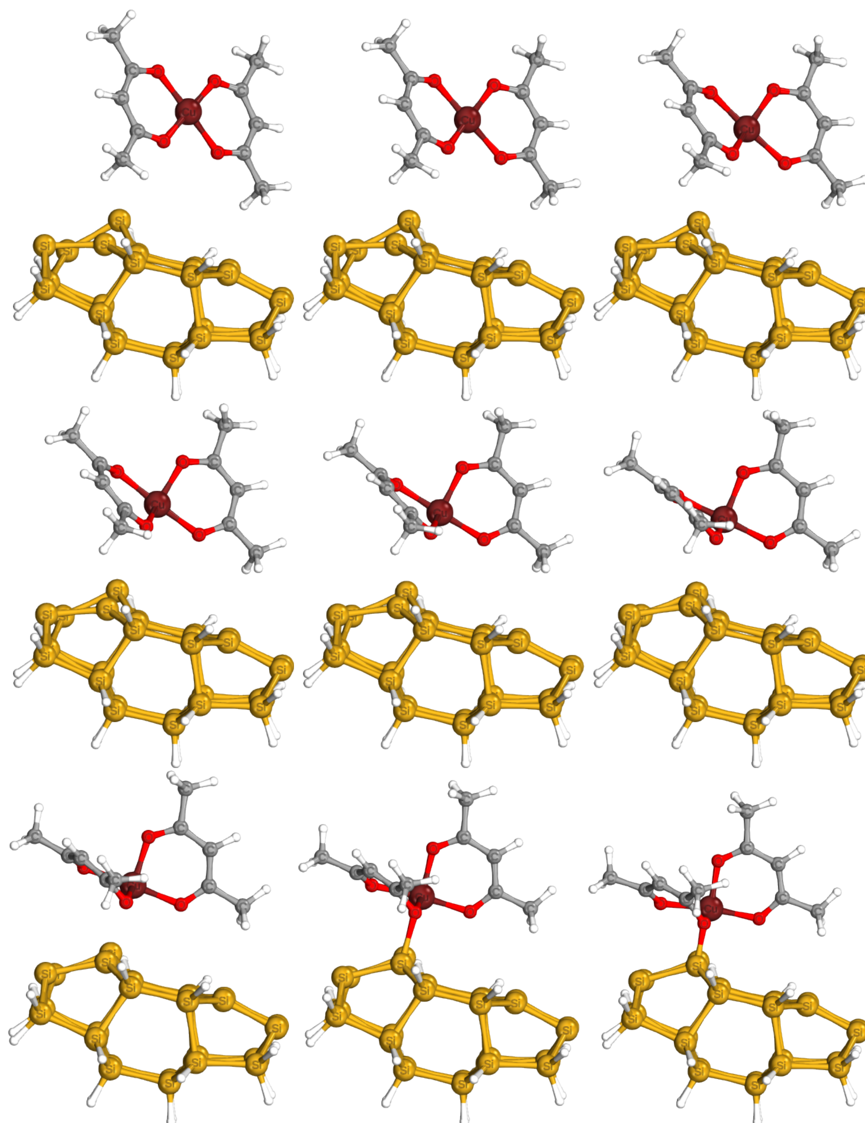

Figure 4.8. Reaction pathway, interpolated images 1 to 9 for Cu precursor reaction on stripped substrate

Starting with the stripped surface configuration, many of the same difficulties were encountered during the simulation, the substrate indeed being too reactive led to having to constrain the precursor during the Geometry Optimization of step 1 (top left corner of 4.8).

The precursor breaks one of its oxygen-copper bonds and they respectively bind with two silicon atoms. The molecule is also subjected to a torsion, the Acetyl groups folding in order to find energetical balance in the structure.

As per the energy pathway 4.9, differently from the gold case, it presents a slight rise in energy around image 5, right before a drastic drop, which is probably the cause of the premature reaction happening during the geometry optimization with the unrestrained precursor. As per what pertains the convergence of the simulation, despite being one of the most lengthy, the NEB section reached convergence without many issues, the same cannot be said for the SCF iteration that reached the maximum allowed number without converging.

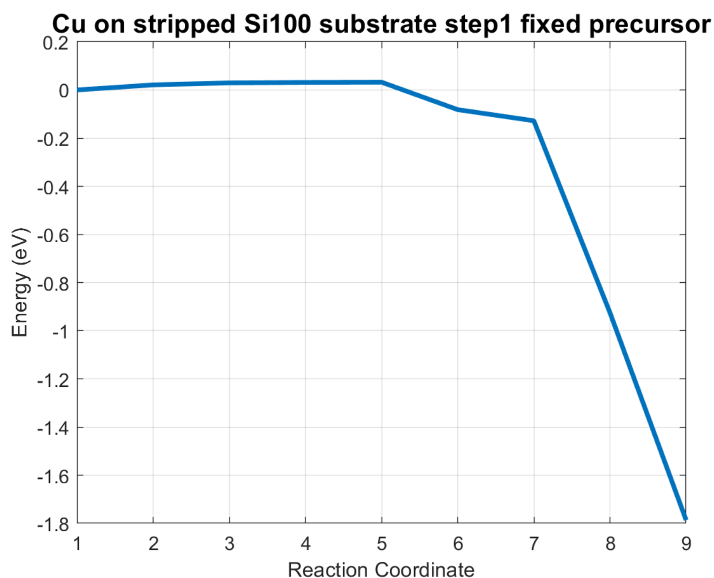

Figure 4.9. Energy pathway of Cu precursor reaction on stripped Si100 substrate (step1 fixed precursor)

Moving on to the passivated structure 4.10, the chemical reaction in the figure involves a hydrogen atom that detaches from the substrate and creates a bond with an oxygen atom that was previously bound to copper, this was deemed the most likely reaction considering that Acetyl groups are very likely to form a hydrogen bond in order to create an Acetylacetone-like molecule, which is a very stable compound.

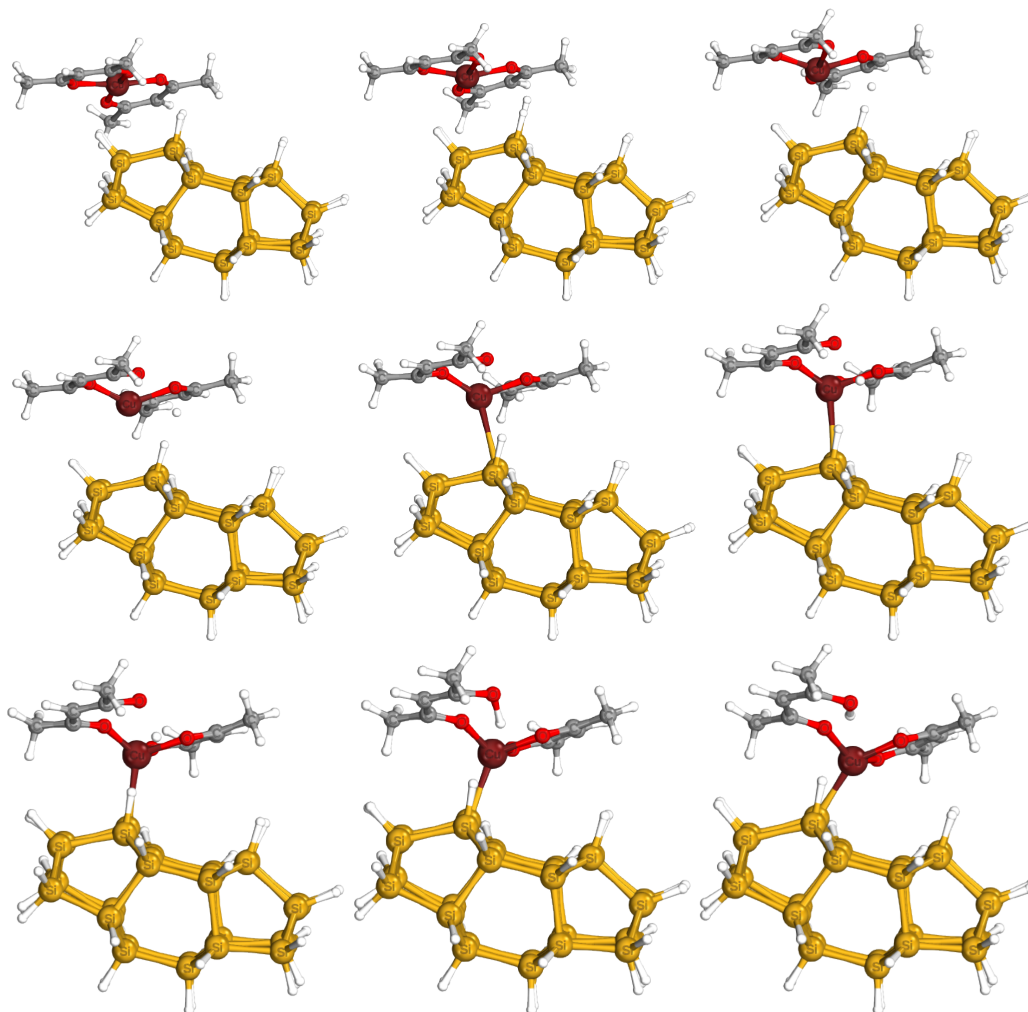

Figure 4.10. Reaction pathway, interpolated images 1 to 9 for Cu precursor reaction on H-passivated substrate

The reaction pathway 4.11 presents a well-pronounced dome-like shape, with a maximum reached around image 5, the last configuration (image 9) has a lower total energy than image 1, a sign that the final state is indeed advantageous and more stable for the structure.

The simulation was convergent both for the NEB section and the SCF cycle and was set up to include counterpoise corrections [55].

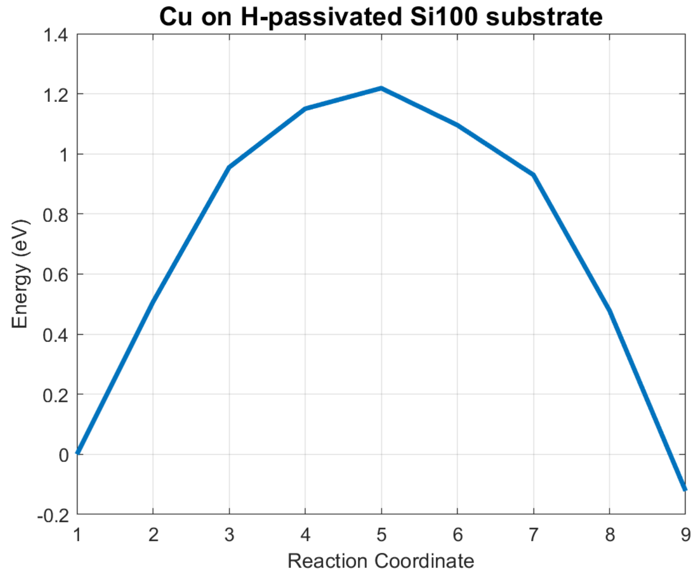

Figure 4.11. Energy pathway of Cu precursor reaction on H-passivated Si100 substrate

The figure 4.12 overlaps both the plot in 4.9 and 4.11, and highlights the rise in energy barrier when dealing with the passivated substrate, again, demonstrating the efficacy of passivation when dealing with deposition selectivity.

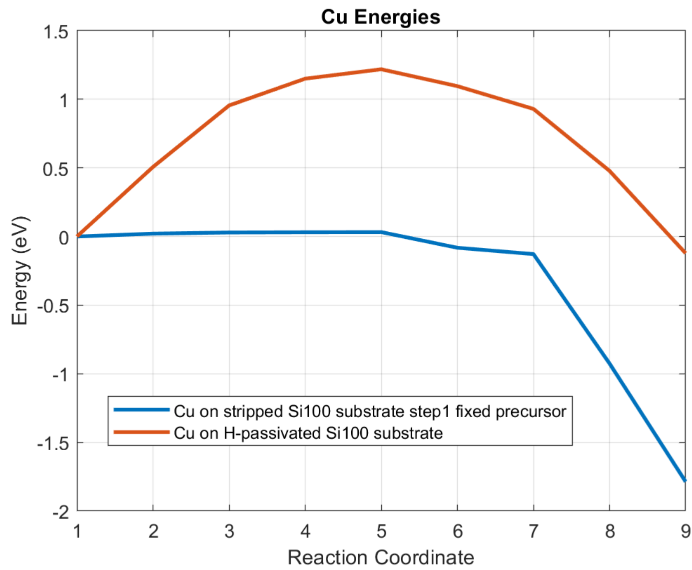

Figure 4.12. Energy pathways comparison for all the Cu reactions: in blue the reaction with the stripped substrate substrate, in orange, the reaction with the H-passivated substrate

It should also be mentioned that there were several trials made with an OH-passivated surface, however, the OH terminations and the precursor don't seem to be compatible, not even during the Geometrical Optimization step, the precursor was subjected to strange torsions and was pushed away from the substrate, and even when trying to force the reactions, the NEB simulation was never successful in converging.

4.1.3 Platinum

The following metal analyzed was platinum, with Trimethyl(methylcyclopentadienyl)platinum(IV) as the precursor of choice.

In figure 4.13 the chemical reaction path for the stripped substrate-precursor interaction is outlined. The first instance portrays, as usual, the precursor hovering over the substrate, this time, however, there were no difficulties in the geometry optimization, attesting to the great stability of the precursor in question.

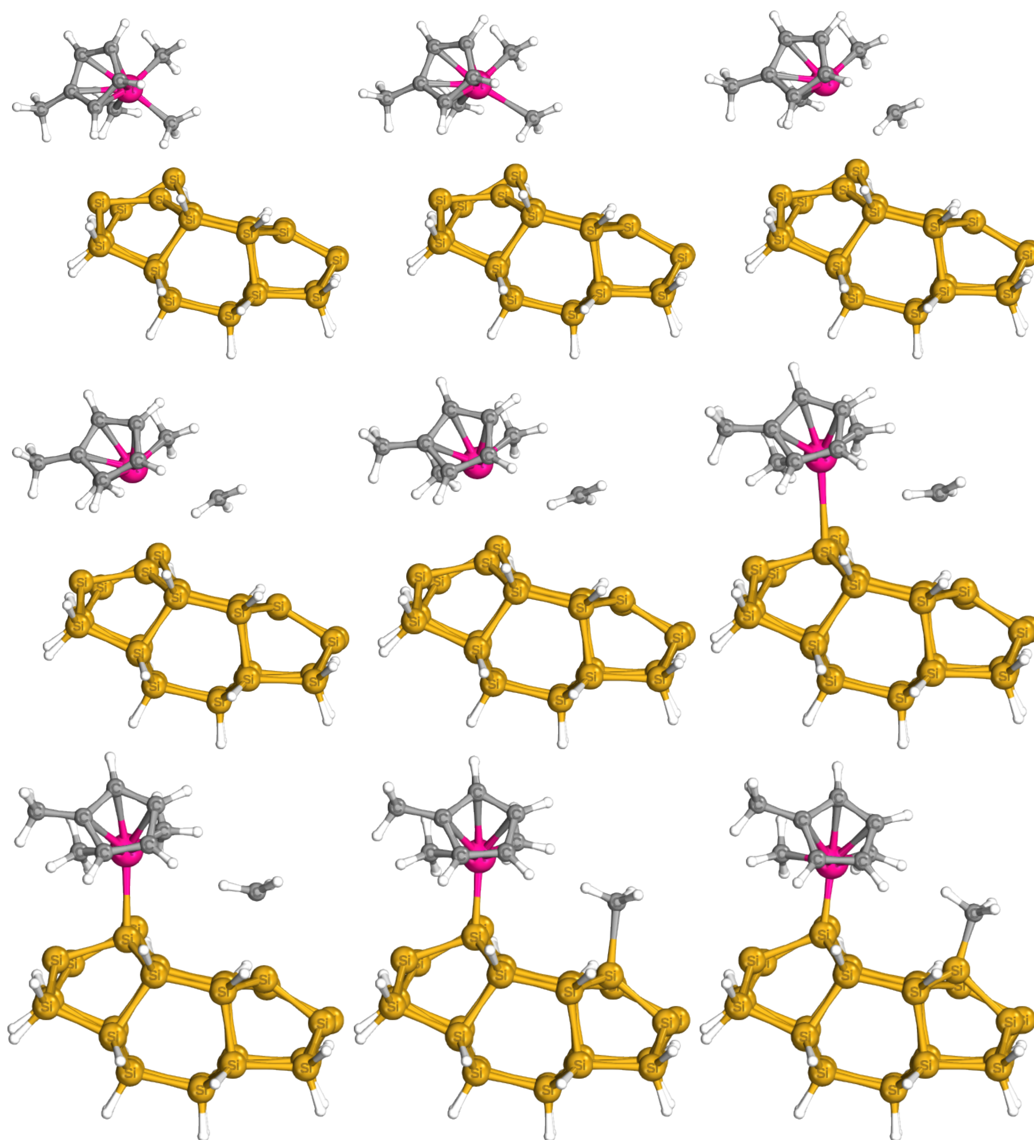

Figure 4.13. Reaction pathway, interpolated images 1 to 9 for Pt precursor reaction on stripped substrate

As shown in the bottom right image of 4.13, in the final configuration the precursor lost one of the methyl groups in order for the platinum to bind to the substrate, and, the roaming CH3 also bonded with one of the available dangling bonds.

In figure 4.13 the reaction pathway for the plotted images is shown, and further corroborates the ease in optimization. The chemical reaction is evidently not spontaneous, however small, there is an energy barrier, although the final image does indeed present as a much lower minimum. The NEB simulation section of the analysis converged, however, the SCF cycle reached the maximum number of iterations, and was unable to terminate.

The energy barrier is to be found around images 3 and 4 and it is greater than the one established for the Copper case 4.8. A much more detailed quantitative analysis can be found in the table 4.1

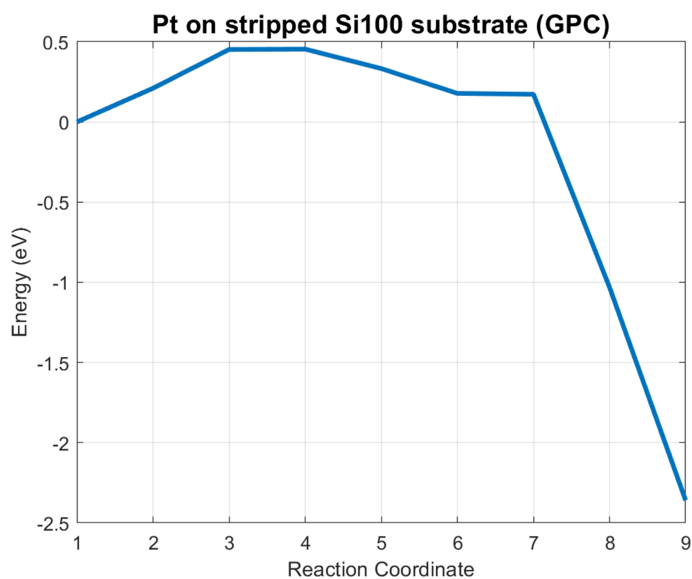

Figure 4.14. Energy pathway of Pt precursor reaction on stripped Si100 substrate (GPC included)

After the energy barrier evaluation for the stripped substrate system, it's time for the passivated substrate-precursor interaction analysis.

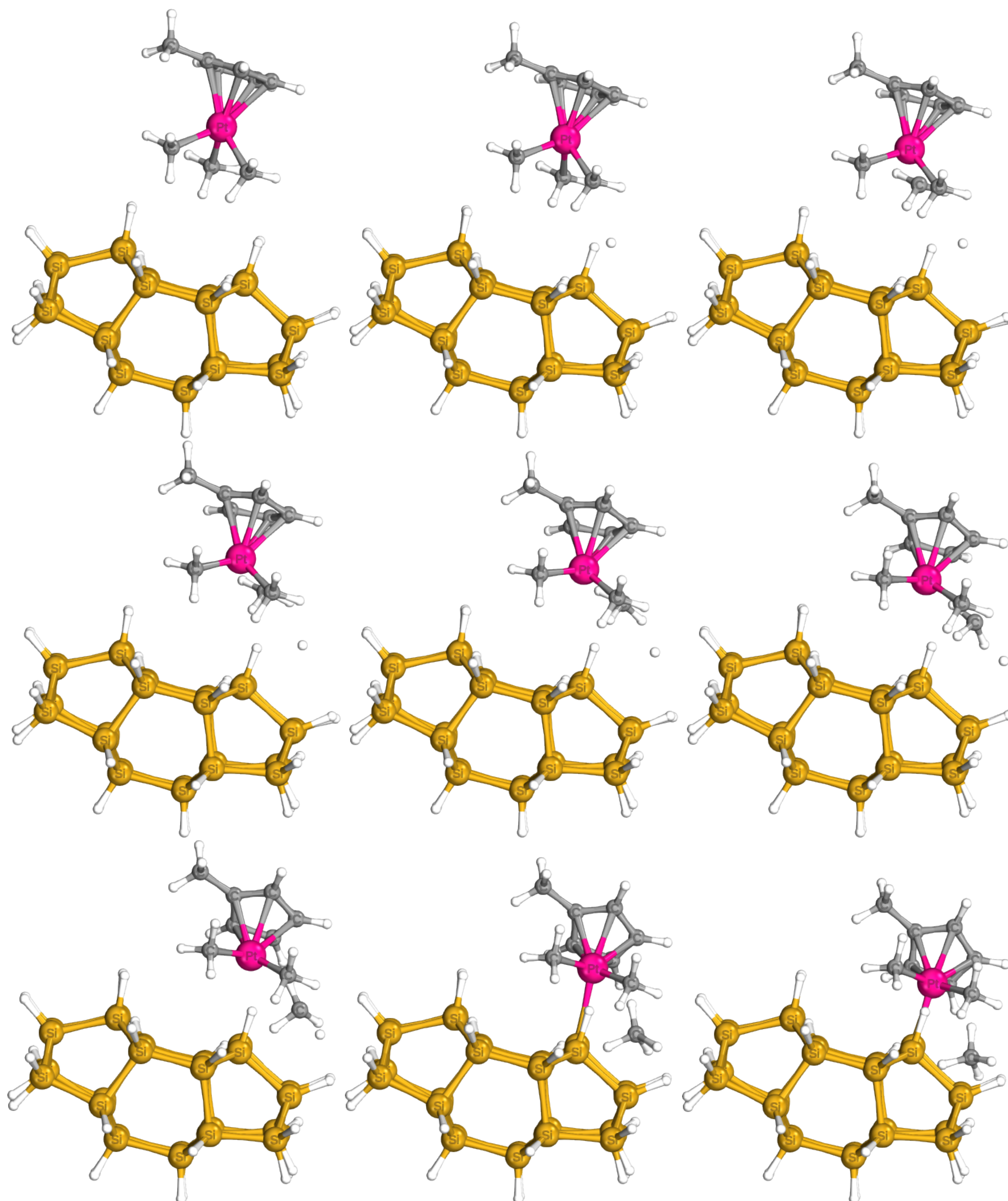

Figure 4.15. Reaction pathway, interpolated images 1 to 9 for Pt precursor reaction on H-passivated substrate (with counterpoise corrections included)

This time in order for the reaction to take place, one of the hydrogen atoms needs to free a silicon dangling bond, this will link with the platinum, and the hydrogen, in combination

with a CH3 will create a CH4 molecule, as sown in 4.15.

The simulation was partially convergent, the NEB terminated successfully, but, the SCF reached the maximum number of iterations without reaching completion.

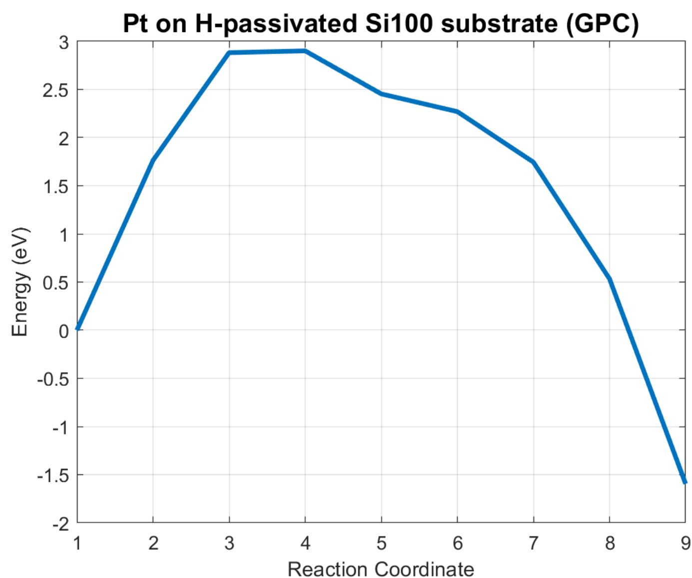

Figure 4.16. Energy pathway of Pt precursor reaction on H-passivated Si100 substrate (GPC included)

In the figure above4.16, the energy curve is shown, the maximum energy is reached between images 3 and 4, and then the plot gradually descends assuming the usual dome shape. The barrier found is quite high, reiterating the validity of the hypothesis.

The setup of this simulation included counterpoise corrections [55], which caused the simulation to treat the platinum as Nikel (a warning much like the one given for gold). This issue arises from the basis set differences. To better gauge how much the counterpoise corrections contribute to the simulation and to better assess the need for their inclusion in the analysis, a simulation excluding them was performed 4.17.

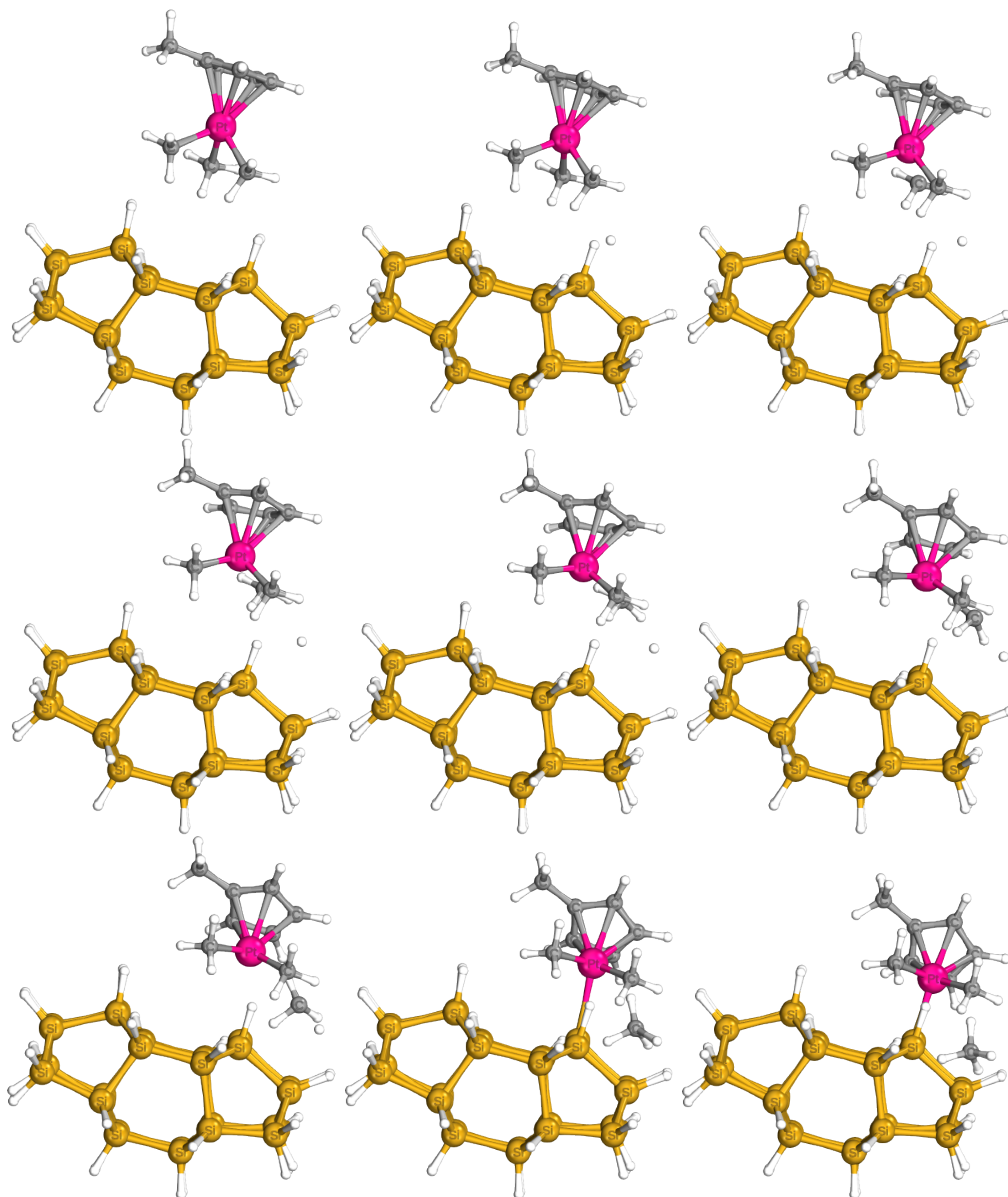

Figure 4.17. Reaction pathway, interpolated images 1 to 9 for Pt precursor reaction on H-passivated substrate (counterpoise corrections not included)

The reaction analyzed in 4.17 is the same as 4.15, with few inevitable variation due to the nature of the coordinate interpolation mechanism.

The results from this simulation are not comparable with the ones including counterpoise corrections.

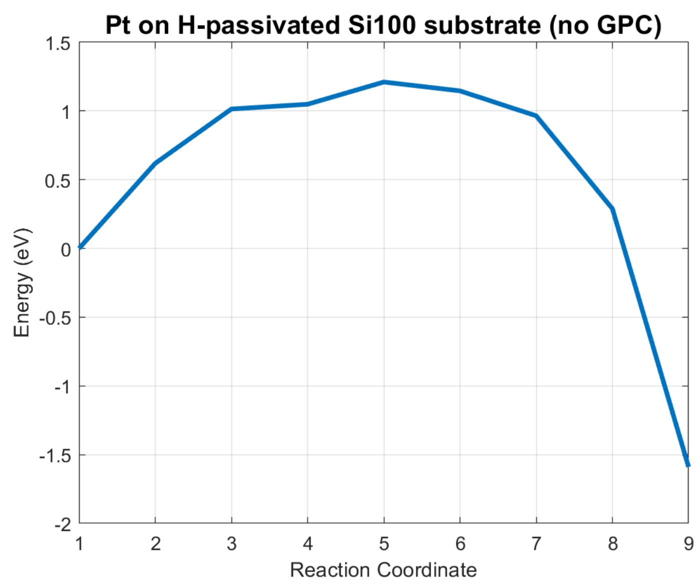

Figure 4.18. Energy pathway of Pt precursor reaction on H-passivated Si100 substrate (GPC not included)

A better comparison can be viewed in figure 4.22.

The last successfully performed simulation was attained on an OH-terminated substrate interacting with the precursor. Platinum was the only metal for which the NEB section of this simulation converged, however, due to some computational difficulties, the SCF cycle never terminated.

The reaction path is shown in the figure below 4.19:

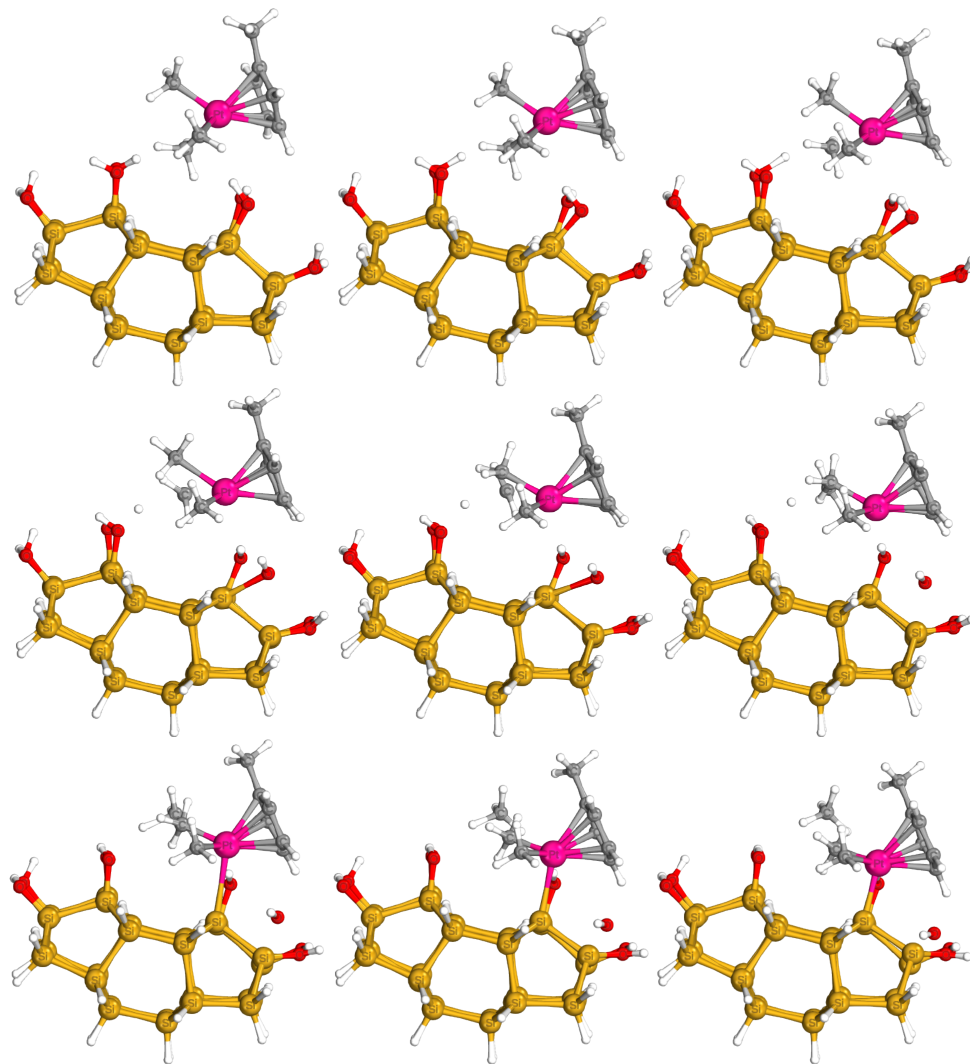

Figure 4.19. Reaction pathway, interpolated images 1 to 9 for Pt precursor reaction on OH-terminated substrate

As shown in figure 4.19, the bonding happens through the detachment of an OH termination from the surface and a methyl group from the precursor, this allows for the platinum to bond with the Silicon.

The reaction pathway has quite a peculiar shape 4.20, it has various local maxima, approximately in image 3, image 5 and image 7, and the final configuration (image 9), has much higher total energy than the first (image 1), hence, the reaction is less likely to happen, since the resulting structure is less energetically efficient.

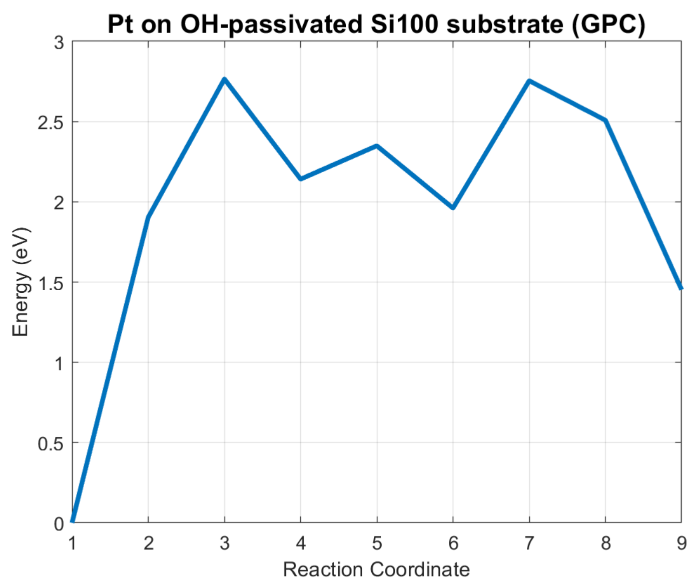

Figure 4.20. Energy pathway of Pt precursor reaction on OH-terminated Si100 substrate

The plot shown next 4.21, better highlights the differences in energy pathways for the different configurations previously laid out.

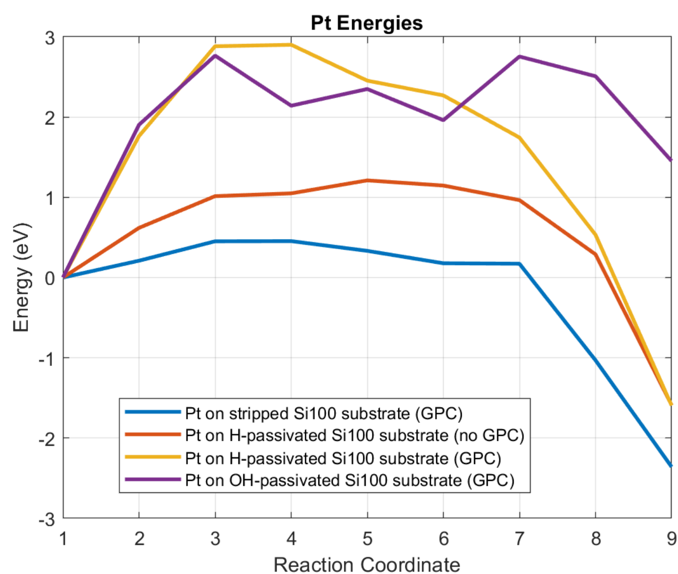

Figure 4.21. Energy pathways comparison for all the Pt reactions: in blue the reaction with the stripped substrate substrate, in yellow, the reaction with the H-passivated substrate including counterpoise corrections, in orange, the reaction with the H-passivated substrate without the inclusion of counterpoise corrections, in purple the reaction with the OH-terminated substrate

The following figure 4.22 instead, underlines the effects of counterpoise corrections.

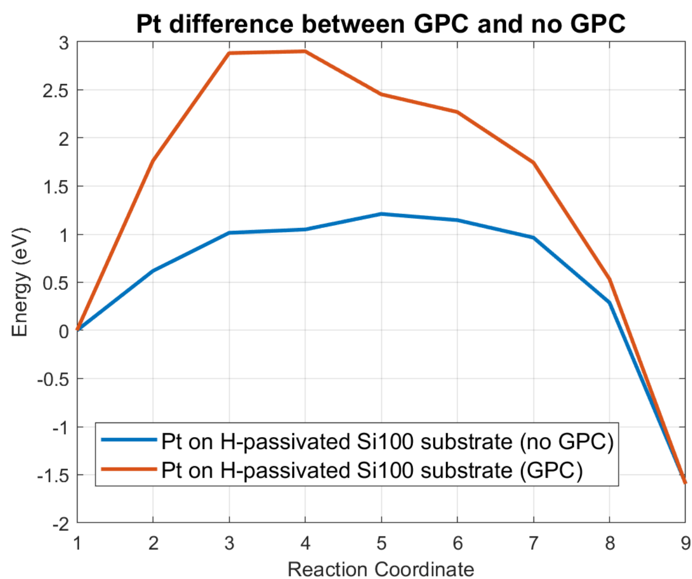

Figure 4.22. Pt - comparison between GPC inclusion (orange line) and no GPC (blue line)

4.1.4 Final Data and Considerations

In conclusion, to have a better picture of the extracted data already graphically portrayed in the figures above, a summary table 4.1 has been exploited. It displays the quantitative results extracted from the discussed simulations. The table is set out to report the Absorption energies that the reaction is set out to have; the absorption energy is defined as :

$$E_{ads} = E_{step1} - E_{Substrate} - E_{Precursor};$$

where the energy for the substrate, for the system in step one and the precursor, were extracted with Matlab exploiting the data from the geometry optimizations performed.

The final energy is the Total energy for the final step of the simulation, and the maximum energy is the value indicating the energy barrier height.

On the table are also reported the energies extracted from the geometry optimizations of the isolated precursors and substrates, this data has been included to justify the much higher values in absorption energies for the Gold processes, indeed the isolated precursor presents with much higher energy. This higher energy state further attests to the lack of stability and explains the difficulties in finding a potential barrier in the reaction with the stripped substrate.
With the extracted data at hand, some considerations need to be made, these results, although in agreement with the initial assumptions, are strongly conditioned by the approximations employed to serve the limits in computational power and by the convergence issues extensively laid out in previous paragraphs.

Ultimately, considering the shown data, in line with the predicted results, the interactions with the passivated silicon substrate always presented a considerably higher energy barrier. This would indicate preferential deposition onto the stripped substrate, hence, when presented with a patterned substrate, the passivated sections (HLD), being there more friction in reacting with the precursors, should effectively act like a mask and induce atomic-scale precision for metal deposition, making selective deposition techniques viable option for nanodevices fabrication.

	Precursor Energy		**Substrate Energy**	**Adsorption Energy**	**Final Energy**	**Maximum Energy** (BARRIER)
Gold	-1.949678401023962e+04	DB	-2.365836495733101e+05	11.328947174835776	-4.121198639452000	0
		H CH4	-2.367196284570907e+05	8.42050115401071	-1.360598027742000	1.794235088546000
		H P		8.42050115401071	0.641181946086000	1.582632983524000
Copper	-6.340821637247538e+04	DB	-2.365836495733101e+05	-0.365511440322734	-1.786415892756000	0.032205508242000
		H	-2.367196284570907e+05	-0.466685306717409	-0.121808294618000	1.218737924578000
Platinum	-1.283363312085408e+04	DB	-2.365836495733101e+05	-0.515593090431139	-2.359113275778000	0.454011596554000
		H GPC	-2.367196284570907e+05	-0.260530080662647	-1.594688177952000	2.900592108036000
		H NO GPC		-0.282854304605280	-1.589527263828000	1.210645798446000
		OH GPC	-2.530957508513692e+05	-0.522150063728986	1.452345888780000	2.764983824022000

Table 4.1. Table reporting the acquired results, extracted from the simulations

4.2 Molecular Dynamics

After having quantitatively demonstrated H-passivation efficiency in masking substrates during Atomic Layer Deposition processes, the next objective is to prove selective deposition techniques efficiency when dealing with less controlled and precise deposition processes like Sputtering.

The choice to simulate sputtering mainly comes from the need for a deposition process that would not require precursors, to better analyze the metal deposition without worrying about byproducts and chemical interactions not directly involved in the deposition. Also, another important factor that skewed the choice was the ability to simulate at a much larger scale, and, a sputtering molecular dynamics simulation would enable it.

The first intention of this study was to set up a large piece of silicon 100 substrate, passivate it with hydrogen atoms, reconstruct its geometry through a geometry optimization process and then design a simple pattern, nanowire shaped, and then proceed to a molecular dynamics simulation of the sputtering process. The expected result would show preferential metal deposition on the stripped section of the substrate.

The simulation was set up through QuantumATK:

- Using the **Builder** tool, a slab of Silicon was sliced along the face 100 (Miller indices indication) through the surface (cleave) function, the lattice size was 8x8x4.
- The substrate was completely passivated 4.23 with the *Passivate the configuration with Hydrogen* function (both the top and bottom, the bottom was passivated to avoid any unwanted interaction and simulate bulk-like behaviour).

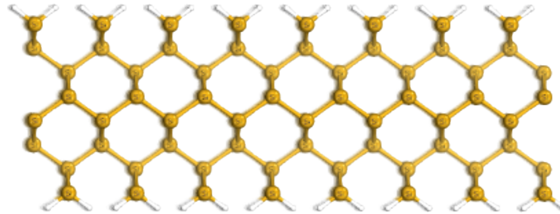

Figure 4.23. Passivated Silicon Slab view from the y-axes direction

- from the face Y of the configuration, alternating rows of Hydrogen atoms were removed 4.24.

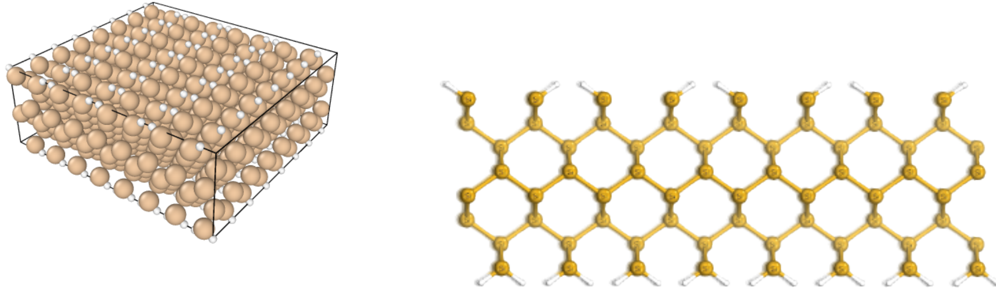

Figure 4.24. Passivated surface with Alternating rows of H removed (oovito view on the left, iboView on the right)

- The configuration was subjected to a geometry optimization, in order to favour surface reconstruction 4.25.

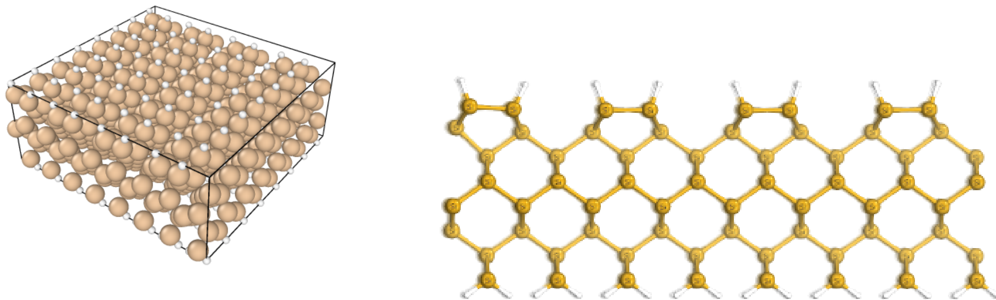

Figure 4.25. Reconstructed and passivated silicon substrate (oovito view on the left, iboView on the right)

- Patterning of the silicon surface (simple nanowire pattern)4.26.

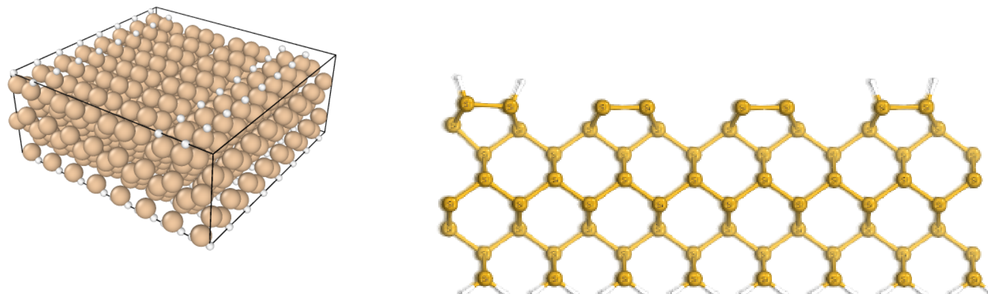

Figure 4.26. Final patterned silicon substrate (oovito view on the left, iboView on the right)

Several trials have been made, however, the limiting factor was the Force Field evaluation, more specifically the force field describing the Cu-H interaction.

4.2.1 MD QuantumATK method

To gain a deeper insight into the issues encountered and the limiting factors for this analysis, it is necessary to have a better understanding of the tools at our disposal.

QuantumATK is able to perform MD simulations but it never could do deposition processes with MD, because the starting geometry had always been fixed to the geometry constructed in the builder given as the input, however, most recently, they added another tool called *multiple surface process* that is based on repetitive iterations of molecular dynamics simulations, and it can effectively reproduce the effects of a sputtering process.

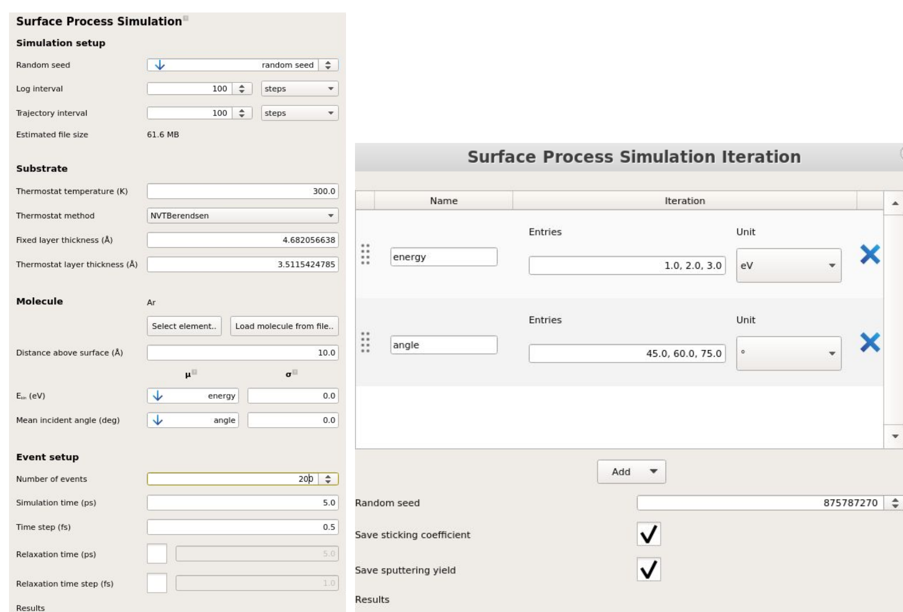

Figure 4.27. GUIs for the multiple process simulation tool setup

For the setup, the desired substrate is needed and can be easily inserted, and then through the GUI, one can choose both the element we wish to deposit and an array of energies and angles at which the deposition will happen, these additional elements (usually in a simulative sputtering process one poses one angle and one energy for the impinging element) provide with some very useful information, for example, 2D plots of the sputtering yield, colour-graded to give a better understanding of the best angle and energy that need to be used for the sputtering process, other than this, the only other data needed is a suitable force field or potential set that can describe the interaction between the elements present in our simulation.

This last step is the hurdle that requires the most attention. QuantumATK comes with a vast collection of potential sets, very few of the potential sets already present included the necessary elements, the sputtering process was meant to be performed for Copper,

hence the required elements were copper, silicon and hydrogen.

Of the four already in the system that can be found in the bibliography [56] [57] [58] [59], only one [56] gave a sensible output, which was still unusable since it disregarded some of the interaction between the atoms, the others outputted an error message, and the simulation was unable to terminate.

Now that the problem was evident, another useful tool was exploited: TremoloX Potential Builder.

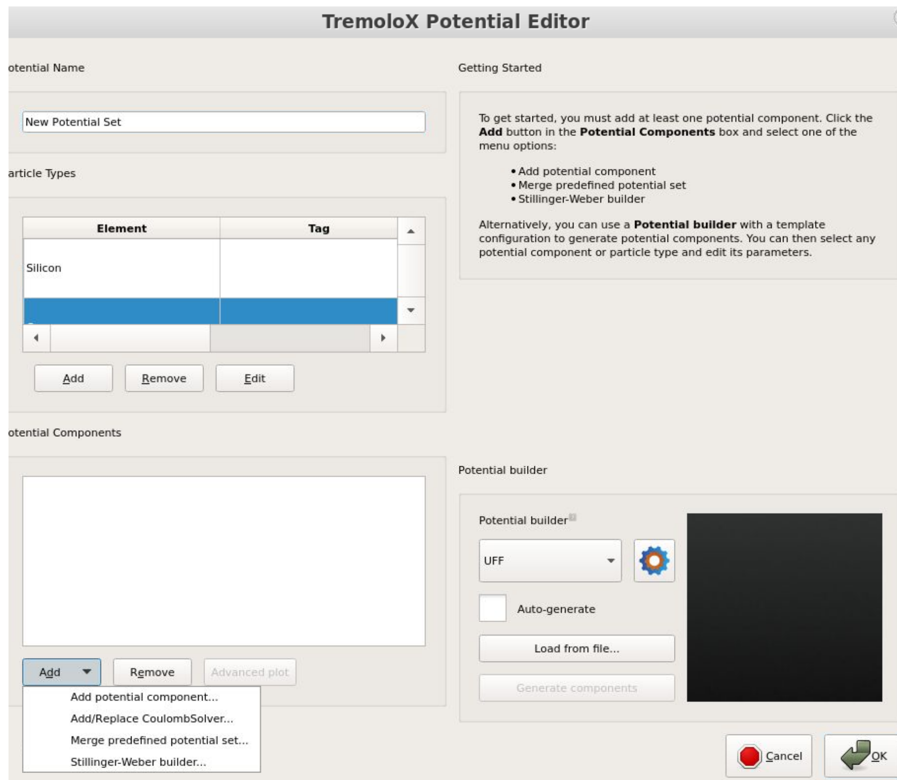

Figure 4.28. GUI for the potential builder TremoloX

This interface was exploited in its entirety, firstly, the *merge* function was used, in order to try and combine some pre-existing potential sets (already included in QuantumATK), several combinations were explored, some would cause errors and abrupt interruptions of the simulations, the most stable combination was between a MEAM [60] set which modelled adequately Copper and Silicon and a Tersoff potential [61] that accounted for Si-H interactions, however, this combination was insufficient since it never accounted for Cu-H potential.

Next, to supply the toll with the missing interaction contributions, several attempts with

some other potential sets were made with some ReaxFF potential sets [62] [63] [64] (some of the resources were found at the link in the bibliography [65]), nonetheless, ReaxFF model doesn't mix well with other types of Force Fields many of these endeavours resulted in errors and simulation crashes.

The last attempts were made exploring the potential builder section of the tool in the bottom left 4.28, a configuration from the **builder** was inserted and the UFF potentials were auto-generated. Unfortunately, these simulations were also unsuccessful.

Despite the many trial runs, none of the combinations of potential sets correctly accounted for the interaction between Cu-H, and if they did, the potentials weren't compatible with each other and the simulation would abruptly be terminated with an error message.

However, to evaluate the actual efficacy of the multiple surface processes tool, a few attempts were conducted with only silicon and copper.

These are the results obtained from the simulation:

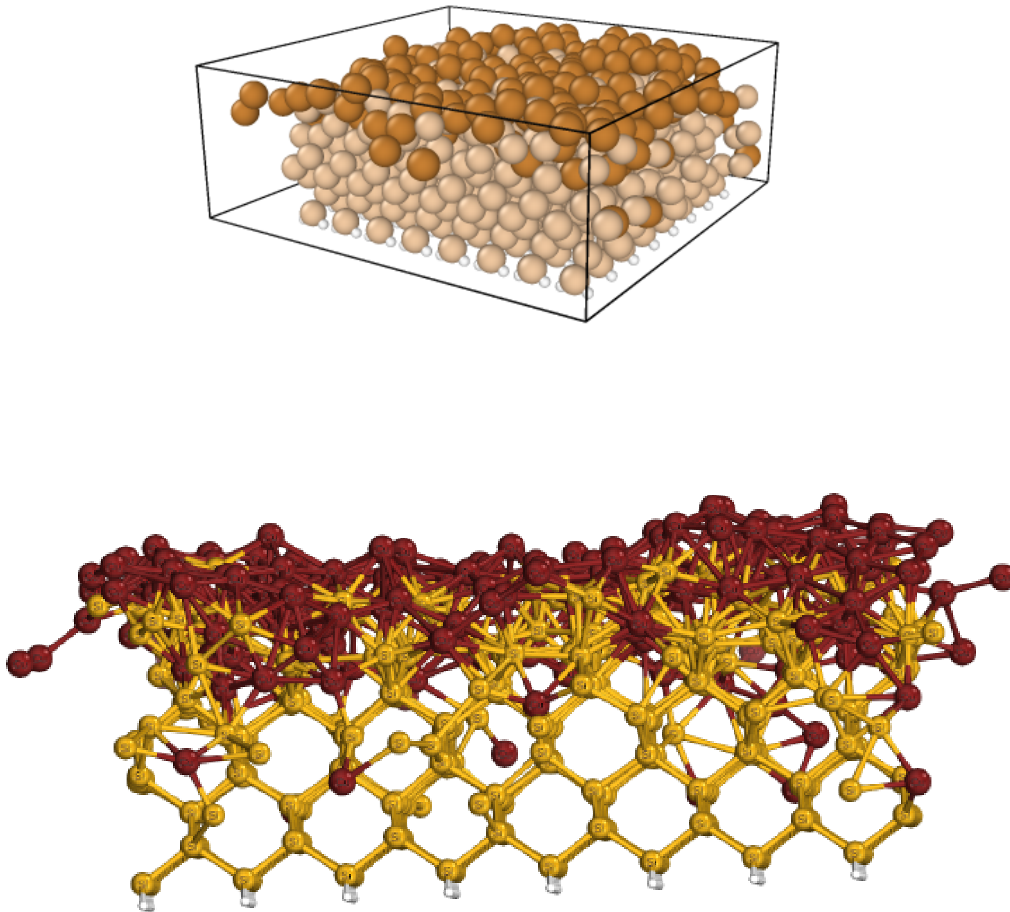

Figure 4.29. MD simulation results, Copper deposition on top of the Si100 substrate, the simulation was run with 200 events (oovito view above, iboView below)

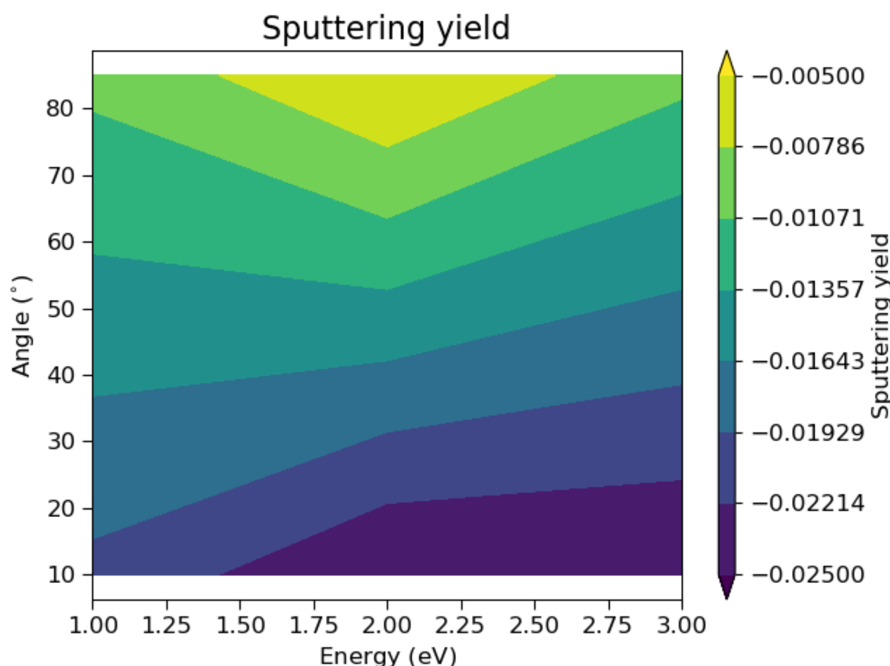

Figure 4.30. 2D plot of the Sputtering Yield

The simulation was carried out with the NVT Beredsen ensemble at 300 K and repeated for 200 deposition events. The deposition angles and energies varied as follows:

- Angle array: $85°, 45°, 10°$
- Energy array: (1, 2, 3) eV

As predicted, the sputtering yield is higher for lower deposition angles and higher energies.

Although no suitable potential set or potential set combination was found, this work was essential in gaining a deeper insight into the inner workings of the tools provided by QuantumATK and provided valuable knowledge on how those tools can be exploited to work around some computational difficulties that other softwares are subjected to. Moreover, another glaring advantage QuantumATK possesses is the ability to perform all the required steps necessary for the setup of a Molecular Dynamic simulation, from the builder, which allows for the geometry creation, to the DFT Geometry Optimization, and the MD simulation in itself, other than providing ease in the post-processing step, since it already yields the necessary extracted data and a suitable GUI, convenient for the visualization of the results.

Chapter 5

Conclusion and future perspectives

This thesis has produced a deep analysis of the inner workings of ALD half-reactions and explored the efficiency of selective deposition techniques like HDL in providing a *mask* layer and improving deposition patterning accuracy. The deposition process has been thoroughly investigated with quantum mechanical *ab initio* simulations with several surface terminations and includes the analysis of several chemical reactions between precursors and substrates. Then, despite the lack of suitable force fields, a larger-scale process was employed to find the suitability of QuantumATK as a tool to perform molecular dynamics simulations. The simulations were able to nicely assess the viability of hydrogen as a passivation layer for a Si100 substrate and predicted an increase in energy barrier that fluctuates between 1.79 and 1.58 eV for Gold, 1.18 eV for Copper and 2.45 eV for Platinum, which is a notable increase in energy for chemical reactions in deposition processes. Next, the exploration of the software QauntumATK allowed for an assessment of its properties and allowed for the extraction of data like Sputtering yield which is usually unviable for MD processes. The extracted quantities were in line with the expectations of a simple sputtering process, which gives a good future perspective on the employment of this tool. Finessing the inputted data or finding a suitable Force Field for the simulation will open new ventures and give even more leeway to Molecular Dynamics analysis.

Nonetheless, this work leaves room for improvement. As mentioned, some of the NEB simulations never reached SCF convergence, and, with more computational power, which indeed was a bit of a limiting factor, some modifications to the convergence conditions and convergence mode can be made to achieve a finished simulation and possibly even more accurate results. Secondly, it would be favourable to address the lack of a suitable Force Field to carry out the larger-scale analysis, so as to have a different model that corroborates hydrogen selectivity.

Conclusively, this work effectively combines *ab initio* quantum mechanical simulations

with Newtonian Molecular Dynamics to both pave better ground for molecular Field-Coupled Nanocomputing devices prototyping and systematically produce selective deposition simulations, hence, advancing one step closer to moving on from the CMOS technology to provide faster and more efficient electronic devices. bridges the simulations to systematically produce selective deposition analysis

Chapter 6

Appendix A

This appendix will provide some code examples for the input files used for the simulations discussed.

For the Geometry Optimizations, an example :

```
    ! PBE opt D3 def2-TZVP GCP(DFT/TZ)

%scf
    scfmode direct
    maxiter 300
end

%pal
    nprocs 6
end

* xyz 0 2
Cu       -1.5879006599     -8.2765653181       3.2191391455
O        -2.7772343369     -9.0790092581       4.4170432654
O        -0.7059047033     -9.7070280481       2.4091667604
O        -2.5497434405     -7.1650066416       2.0807939104
O        -0.3721048329     -7.1462596314       4.0923598057
C        -1.0907544121    -10.9513376823       2.7832841473
C        -2.2922495968    -11.1653257193       3.3601558121
C        -3.2994672461    -10.0616772751       3.5768330990
C        -4.6289908319    -10.5669268636       4.1188729748
H        -5.3409717877     -9.7180130262       4.1936163889
H        -4.4944274698    -11.0214981640       5.1226942258
H        -5.0566767982    -11.3208910544       3.4242748803
C        -0.1577278671    -12.1042943838       2.5567153098
H        -0.6357433637    -12.8613553511       1.9000301952
H         0.0951780343    -12.5761588628       3.5309760590
H         0.7821871491    -11.7557831862       2.0800696070
C        -2.2518173226     -5.8476173063       2.1201471319
C         0.0418788338     -6.3482128052       3.0235829987
```

```
C       -1.0620257667     -5.4128548294       2.5844900660
C       -3.2814961624     -4.8603738321       1.6568750817
H       -2.8831469994     -4.2528670396       0.8179528337
H       -3.5568922943     -4.1882800424       2.4981801885
H       -4.1970152580     -5.3890648411       1.3169444803
C        1.3167853943     -5.5990789955       3.3928255588
H        1.6589298222     -4.9865335613       2.5312515194
H        2.1163683115     -6.3273375594       3.6428890028
H        1.1400417170     -4.9363729836       4.2664477403
H       -0.8725564859     -4.3417500172       2.6085985227
H       -2.5637671561    -12.1786651963       3.6491205929

*
```

The coordinates reported refer to the chosen precursor for copper and should be substituted with the needed coordinates for the system in analysis.

NEB simulation setup example :

```
    ! PBE D3 def2-TZVP GCP(DFT/TZ) NEB-TS
%scf
    scfmode direct
    maxiter 300
end
%pal
    nprocs 12
end

%geom
    Constraints
        {C 8:51 C}
    end
end

%neb
    neb_end_xyzfile "step1_Si_Cu.xyz"
    nimages 7
    maxiter 1000
end
* xyzfile 0 2 step0_Si_Cu.xyz
```

Here, again the name for the input and output configurations change with the different simulation types.

As per what concerns the post-processing, the implemented Matlab codes will roughly show how the data extraction was executed.

```
%Cu
% Neb_SiCu
fd = fileread("C:\Users\mrz-b\Desktop\poli\00_tesi\my_NEB\Cu\Cuacac2\cuacac2.engrad");
Precursor= regexp(fd, "\s\s(-*\d+.\d+)",'tokens');
Precursor_En = str2double(cell2mat(Precursor{1}))*ConvConst;

fd1 = fileread("C:\Users\mrz-b\Desktop\poli\00_tesi\my_NEB\Cu\Si_substrate\
Si_substrate.engrad");
Substrate= regexp(fd1, "\s\s(-*\d+.\d+)",'tokens');
Substrate_En = str2double(cell2mat(Substrate{1}))*ConvConst;

fd2 = fileread("C:\Users\mrz-b\Desktop\poli\00_tesi\my_NEB\Cu\0_Si_Cuacac2\
step0_Si_Cu.engrad");
Step1= regexp(fd2, "\s\s(-*\d+.\d+)",'tokens');
Step1_En = str2double(cell2mat(Step1{1}))*ConvConst;
AdsorptionEnergy = Step1_En - Substrate_En - Precursor_En;

% NEB
fileInterp = fileread("C:\Users\mrz-b\Desktop\poli\00_tesi\my_NEB\Cu\NEB_SiCu\
neb_Cu.final.interp");
ImageEnergies= regexp(fileInterp, "(\d.\d+)\s+(\d+.\d+)\s+([+-]?\d.\d+)\s+",'tokens');
ii = 1; imNum = 0;
while(imNum ~= 1)
    imNum = str2double(cell2mat(ImageEnergies{ii}(1)));
    imEn(ii) = str2double(cell2mat(ImageEnergies{ii}(3)));
    ii = ii+1;
end
FinalEnergy= imEn(length(imEn))*ConvConst;
TS_En = max(imEn);
TS_En(1) = TS_En*ConvConst;
%print reaction Coordinate
imEn = imEn.*ConvConst;
reactCoord = linspace(1,length(imEn),length(imEn));
figure()
plot(reactCoord, imEn, 'LineWidth', 2.5)
grid on
box on
title("Cu on stripped Si100 substrate step1 fixed precursor",'fontname', "Helvetica",
'fontsize',14)
xlabel("Reaction Coordinate")
ylabel("Energy (eV)")
```

Of course, the file directories are unique to each calculator. Several codes were exploited to extract the necessary data, this served as a sample of the main structure.

Bibliography

[1] Yuri Ardesi, Umberto Garlando, Fabrizio Riente, Giuliana Beretta, Gianluca Piccinini, and Mariagrazia Graziano. Taming molecular field-coupling for nanocomputing design. *ACM Journal on Emerging Technologies in Computing Systems*, 19(1):1–24, 2022.

[2] Ruan Evangelista Formigoni, Ricardo Santos Ferreira, and José Augusto M Nacif. A survey on placement and routing for field-coupled nanocomputing. *Journal of Integrated Circuits and Systems*, 16(1):1–9, 2021.

[3] Jaehong Lee, Jaehong Yoon, Hyun Gu Kim, Subin Kang, Woo-Suk Oh, Hassan Algadi, Saleh Al-Sayari, Bonggeun Shong, Soo-Hyun Kim, Hyungjun Kim, et al. Highly conductive and flexible fiber for textile electronics obtained by extremely low-temperature atomic layer deposition of pt. *NPG Asia Materials*, 8(11):e331–e331, 2016.

[4] Alan J Elliot, Gary Malek, Logan Wille, Rongtao Lu, Siyuan Han, Judy Z Wu, John Talvacchio, and Rupert M Lewis. Probing the nucleation of al_2o_3 in atomic layer deposition on aluminum for ultrathin tunneling barriers in josephson junctions. *IEEE transactions on applied superconductivity*, 23(3):1101405–1101405, 2013.

[5] Jani Hamalainen, Mikko Ritala, and Markku Leskela. Atomic layer deposition of noble metals and their oxides. *Chemistry of Materials*, 26(1):786–801, 2014.

[6] Yasumitsu Miyata. Cvd growth of atomically-thin transition metal dichalcogenides and their heterostructures. In *JSAP Annual Meetings Extended Abstracts*, pages 124–124. The Japan Society of Applied Physics, 2016.

[7] Masato M Maitani and David L Allara. Issues and challenges in vapor-deposited top metal contacts for molecule-based electronic devices. *Unimolecular and Supramolecular Electronics I: Chemistry and Physics Meet at Metal-Molecule Interfaces*, pages 239–273, 2012.

[8] Michiel Van Daele, Matthew BE Griffiths, Matthias M Minjauw, Seán T Barry, Christophe Detavernier, and Jolien Dendooven. Reaction mechanism of the me 3 aupme 3–h 2 plasma-enhanced ald process. *Physical Chemistry Chemical Physics*, 22(21):11903–11914, 2020.

[9] Fatemeh SM Hashemi, Fabio Grillo, Vikram R Ravikumar, Dominik Benz, Ankit Shekhar, Matthew BE Griffiths, Seán T Barry, and J Ruud Van Ommen. Thermal atomic layer deposition of gold nanoparticles: controlled growth and size selection for photocatalysis. *Nanoscale*, 12(16):9005–9013, 2020.

[10] Titta Aaltonen, Antti Rahtu, Mikko Ritala, and Markku Leskelä. Reaction mechanism studies on atomic layer deposition of ruthenium and platinum. *Electrochemical*

and solid-state letters, 6(9):C130, 2003.

[11] Adriaan JM Mackus, Diana Garcia-Alonso, Harm CM Knoops, Ageeth A Bol, and Wilhelmus MM Kessels. Room-temperature atomic layer deposition of platinum. *Chemistry of Materials*, 25(9):1769–1774, 2013.

[12] HCM Knoops, AJM Mackus, ME Donders, MCM Van De Sanden, PHL Notten, and WMM Kessels. Remote plasma ald of platinum and platinum oxide films. *Electrochemical and Solid-State Letters*, 12(7):G34, 2009.

[13] Luca Magagnin, R Maboudian, and C Carraro. Selective deposition of thin copper films onto silicon with improved adhesion. *Electrochemical and Solid-State Letters*, 4(1):C5, 2000.

[14] Mari Endresen Alnes, Edouard Monakhov, Helmer Fjellvåg, and Ola Nilsen. Atomic layer deposition of copper oxide using copper (ii) acetylacetonate and ozone. *Chemical Vapor Deposition*, 18(4-6):173–178, 2012.

[15] Zahra Golrokhi, Paul A Marshall, Simon Romani, Simon Rushworth, Paul R Chalker, and Richard J Potter. The influence of tertiary butyl hydrazine as a co-reactant on the atomic layer deposition of silver. *Applied Surface Science*, 399:123–131, 2017.

[16] JW Elam, A Zinovev, CY Han, HH Wang, U Welp, JN Hryn, and MJ Pellin. Atomic layer deposition of palladium films on al2o3 surfaces. *Thin Solid Films*, 515(4):1664–1673, 2006.

[17] Young-Soon Kim, Jiho Shin, Joong-Hee Cho, Gregory A Ten Eyck, De-Li Liu, Samuk Pimanpang, Toh-Ming Lu, Jay J Senkevich, and Hyung-Shik Shin. Surface characterization of copper electroless deposition on atomic layer deposited palladium on iridium and tungsten. *Surface and Coatings Technology*, 200(20-21):5760–5766, 2006.

[18] Gregory A Ten Eyck, Samuk Pimanpang, Jasbir S Juneja, Hassaram Bakhru, T-M Lu, and G-C Wang. Plasma-enhanced atomic layer deposition of palladium on a polymer substrate. *Chemical vapor deposition*, 13(6-7):307–311, 2007.

[19] Ji-Yu Feng, Matthias M Minjauw, Ranjith K Ramachandran, Michiel Van Daele, Hilde Poelman, Timo Sajavaara, Jolien Dendooven, and Christophe Detavernier. The co-reactant role during plasma enhanced atomic layer deposition of palladium. *Physical Chemistry Chemical Physics*, 22(16):9124–9136, 2020.

[20] JHG Owen. Chemical routes for transfer of atomic-scale patterns. 2018.

[21] Taleana Huff, Hatem Labidi, Mohammad Rashidi, Lucian Livadaru, Thomas Dienel, Roshan Achal, Wyatt Vine, Jason Pitters, and Robert A Wolkow. Binary atomic silicon logic. *Nature Electronics*, 1(12):636–643, 2018.

[22] John N Randall, Joseph W Lyding, S Schmucker, James R Von Ehr, Joshua Ballard, Rahul Saini, Hai Xu, and Yinong Ding. Atomic precision lithography on si. *Journal of Vacuum Science & Technology B: Microelectronics and Nanometer Structures Processing, Measurement, and Phenomena*, 27(6):2764–2768, 2009.

[23] Jason Pitters, Jeremiah Croshaw, Roshan Achal, Lucian Livadaru, Samuel Ng, Robert Lupoiu, Taras Chutora, Taleana Huff, Konrad Walus, and Robert A Wolkow. Atomically precise manufacturing of silicon electronics. *ACS nano*, 2024.

[24] Robert A Wolkow, Lucian Livadaru, Jason Pitters, Marco Taucer, Paul Piva, Mark Salomons, Martin Cloutier, and Bruno VC Martins. Silicon atomic quantum dots enable beyond-cmos electronics. *Field-Coupled Nanocomputing: Paradigms, Progress,*

and Perspectives, pages 33–58, 2014.

[25] Niko Pavliček, Zsolt Majzik, Gerhard Meyer, and Leo Gross. Tip-induced passivation of dangling bonds on hydrogenated si (100)-2× 1. *Applied Physics Letters*, 111(5), 2017.

[26] KJ Dwyer, Michael Dreyer, and RE Butera. Stm-induced desorption and lithographic patterning of cl–si (100)-(2× 1). *The Journal of Physical Chemistry A*, 123(50):10793–10803, 2019.

[27] Matthias Müllenborn, Karen Birkelund, Francois Grey, and Steen Madsen. Laser direct writing of oxide structures on hydrogen-passivated silicon surfaces. *Applied physics letters*, 69(20):3013–3015, 1996.

[28] Yaoqiao Hu, Pak San Yip, Chak Wah Tang, Kei May Lau, and Qiang Li. Interface passivation and trap reduction via hydrogen fluoride for molybdenum disulfide on silicon oxide back-gate transistors. *Semiconductor Science and Technology*, 33(4):045005, 2018.

[29] Jonathan Wyrick, Xiqiao Wang, Pradeep Namboodiri, Ranjit Vilas Kashid, Fan Fei, Joseph Fox, and Richard Silver. Enhanced atomic precision fabrication by adsorption of phosphine into engineered dangling bonds on h–si using stm and dft. *ACS nano*, 16(11):19114–19123, 2022.

[30] JN Randall, JB Ballard, JW Lyding, S Schmucker, JR Von Ehr, R Saini, H Xu, and Y Ding. Atomic precision patterning on si: An opportunity for a digitized process. *Microelectronic engineering*, 87(5-8):955–958, 2010.

[31] John N Randall, James HG Owen, Ehud Fuchs, Rahul Saini, Robin Santini, and SOR Moheimani. Atomically precise digital e-beam lithography. In *Novel Patterning Technologies for Semiconductors, MEMS/NEMS and MOEMS 2020*, volume 11324, pages 116–127. SPIE, 2020.

[32] John N Randall, James HG Owen, Joseph Lake, Rahul Saini, Ehud Fuchs, Mohammad Mahdavi, SO Moheimani, and Benjamin Carrion Schaefer. Highly parallel scanning tunneling microscope based hydrogen depassivation lithography. *Journal of Vacuum Science & Technology B*, 36(6), 2018.

[33] Joshua B Ballard, Thomas W Sisson, James HG Owen, William R Owen, Ehud Fuchs, Justin Alexander, John N Randall, and James R Von Ehr. Multimode hydrogen depassivation lithography: A method for optimizing atomically precise write times. *Journal of Vacuum Science & Technology B*, 31(6), 2013.

[34] Ehud Fuchs. Identifying surface elements in stm images using neural networks. In *Optical Fibers and Sensors for Medical Diagnostics, Treatment and Environmental Applications XXI*, volume 11635, page 116350W. SPIE, 2021.

[35] Joshua B Ballard, James HG Owen, William Owen, Justin R Alexander, Ehud Fuchs, John N Randall, James R Von Ehr, Stephen McDonnell, Don D Dick, Robert M Wallace, et al. Pattern transfer of hydrogen depassivation lithography patterns into silicon with atomically traceable placement and size control. *Journal of Vacuum Science & Technology B*, 32(4), 2014.

[36] DP Adams, TM Mayer, and BS Swartzentruber. Selective area growth of metal nanostructures. *Applied physics letters*, 68(16):2210–2212, 1996.

[37] KEJ Goh, S Chen, H Xu, J Ballard, JN Randall, and JR Von Ehr. Using patterned

h-resist for controlled three-dimensional growth of nanostructures. *Applied Physics Letters*, 98(16), 2011.

[38] Wolfram Koch and Max C Holthausen. *A chemist's guide to density functional theory*. John Wiley & Sons, 2015.

[39] Walter Kohn, Axel D Becke, and Robert G Parr. Density functional theory of electronic structure. *The journal of physical chemistry*, 100(31):12974–12980, 1996.

[40] Pierre Hohenberg and Walter Kohn. Inhomogeneous electron gas. *Physical review*, 136(3B):B864, 1964.

[41] Vilhjálmur Ásgeirsson, Benedikt Orri Birgisson, Ragnar Bjornsson, Ute Becker, Frank Neese, Christoph Riplinger, and Hannes Jónsson. Nudged elastic band method for molecular reactions using energy-weighted springs combined with eigenvector following. *Journal of Chemical Theory and Computation*, 17(8):4929–4945, 2021.

[42] Shūichi Nosé. A molecular dynamics method for simulations in the canonical ensemble. *Molecular physics*, 52(2):255–268, 1984.

[43] Loup Verlet. Computer" experiments" on classical fluids. i. thermodynamical properties of lennard-jones molecules. *Physical review*, 159(1):98, 1967.

[44] Hans C Andersen. Molecular dynamics simulations at constant pressure and/or temperature. *The Journal of chemical physics*, 72(4):2384–2393, 1980.

[45] Daan Frenkel and Berend Smit. *Understanding molecular simulation: from algorithms to applications*. Elsevier, 2023.

[46] Judith A Harrison, J David Schall, Sabina Maskey, Paul T Mikulski, M Todd Knippenberg, and Brian H Morrow. Review of force fields and intermolecular potentials used in atomistic computational materials research. *Applied Physics Reviews*, 5(3), 2018.

[47] Avogadro. `https://avogadro.cc/`.

[48] Orca. `https://www.orcasoftware.de/tutorials_orca/index.html`.

[49] Florian Weigend. Accurate coulomb-fitting basis sets for h to rn. *Physical chemistry chemical physics*, 8(9):1057–1065, 2006.

[50] Florian Weigend and Reinhart Ahlrichs. Balanced basis sets of split valence, triple zeta valence and quadruple zeta valence quality for h to rn: Design and assessment of accuracy. *Physical Chemistry Chemical Physics*, 7(18):3297–3305, 2005.

[51] John P Perdew, Kieron Burke, and Matthias Ernzerhof. Generalized gradient approximation made simple. *Physical review letters*, 77(18):3865, 1996.

[52] Stefan Grimme, Jens Antony, Stephan Ehrlich, and Helge Krieg. A consistent and accurate ab initio parametrization of density functional dispersion correction (dft-d) for the 94 elements h-pu. *The Journal of Chemical Physics*, 132(15):154104, 2010.

[53] Stefan Grimme, Stephan Ehrlich, and Lars Goerigk. Effect of the damping function in dispersion corrected density functional theory. *Journal of Computational Chemistry*, 32(7):1456–1465, 2011.

[54] F Weigend and R Ahlrichs. Phys chem chem phys 7: 3297, 2005.

[55] Holger Kruse and Stefan Grimme. A geometrical correction for the inter-and intramolecular basis set superposition error in hartree-fock and density functional theory calculations for large systems. *The Journal of chemical physics*, 136(15), 2012.

[56] Adam Lloyd, David Cornil, ACT Van Duin, Diana van Duin, Roger Smith,

SD Kenny, Jérôme Cornil, and David Beljonne. Development of a reaxff potential for ag/zn/o and application to ag deposition on zno. *Surface Science*, 645:67–73, 2016.

[57] Kevin D Nielson, Adri CT Van Duin, Jonas Oxgaard, Wei-Qiao Deng, and William A Goddard. Development of the reaxff reactive force field for describing transition metal catalyzed reactions, with application to the initial stages of the catalytic formation of carbon nanotubes. *The Journal of Physical Chemistry A*, 109(3):493–499, 2005.

[58] George M Psofogiannakis, John F McCleerey, Eugenio Jaramillo, and Adri CT Van Duin. Reaxff reactive molecular dynamics simulation of the hydration of cu-ssz-13 zeolite and the formation of cu dimers. *The Journal of Physical Chemistry C*, 119(12):6678–6686, 2015.

[59] Amar M Kamat, Adri CT Van Duin, and Alexei Yakovlev. Molecular dynamics simulations of laser-induced incandescence of soot using an extended reaxff reactive force field. *The Journal of Physical Chemistry A*, 114(48):12561–12572, 2010.

[60] Bohumir Jelinek, Sebastien Groh, Mark F Horstemeyer, Jeffery Houze, Seong-Gon Kim, Gregory J Wagner, Amitava Moitra, and Michael I Baskes. Modified embedded atom method potential for al, si, mg, cu, and fe alloys. *Physical Review B*, 85(24):245102, 2012.

[61] F de Brito Mota, JF Justo, and Adalberto Fazzio. Hydrogen role on the properties of amorphous silicon nitride. *Journal of applied physics*, 86(4):1843–1847, 1999.

[62] Kamyar Akbari Roshan, Mahdi Khajeh Talkhoncheh, Jonathan E Mueller, William A Goddard III, and Adri CT van Duin. Development of the reaxff reactive force field for cu/si systems with application to copper cluster formation during cu diffusion inside silicon. *The Journal of Physical Chemistry C*, 125(35):19455–19466, 2021.

[63] Shuodong Mi, Cheng Bao, and Xin Lv. Reaxff reactive molecular dynamics study on electrochemistry of h2/co hybrid fuel in ni/ysz anode. *Fuel*, 332:125989, 2023.

[64] Jialin Wen, Tianbao Ma, Weiwei Zhang, George Psofogiannakis, Adri CT van Duin, Lei Chen, Linmao Qian, Yuanzhong Hu, and Xinchun Lu. Atomic insight into tribochemical wear mechanism of silicon at the si/sio2 interface in aqueous environment: Molecular dynamics simulations using reaxff reactive force field. *Applied Surface Science*, 390:216–223, 2016.

[65] Software for chemistry and materials. `https://www.scm.com/`.

[66] Yuri Ardesi, Alessandro Gaeta, Giuliana Beretta, Gianluca Piccinini, and Mariagrazia Graziano. Ab initio molecular dynamics simulations of field-coupled nanocomputing molecules. *Journal of Integrated Circuits and Systems*, 16(1):1–8, 2021.

[67] Mariagrazia Graziano, Ruiyu Wang, Massimo Ruo Roch, Yuri Ardesi, Fabrizio Riente, and Gianluca Piccinini. Characterisation of a bis-ferrocene molecular qca wire on a non-ideal gold surface. *Micro & Nano Letters*, 14(1):22–27, 2019.

[68] Marek Kolmer and Christian Joachim. *On-Surface Atomic Wires and Logic Gates*. Springer, 2017.

[69] Ruwani N Wasalathanthri, Yukun Gong, Monika M Biener, Anna N Ivanovskaya,

Nikola A Dudukovic, and Rohan Akolkar. Adsorption processes during electrochemical atomic layer deposition of gold. *Journal of The Electrochemical Society*, 168(11):112505, 2021.

[70] Michiel Van Daele, Matthew BE Griffiths, Ali Raza, Matthias M Minjauw, Eduardo Solano, Ji-Yu Feng, Ranjith K Ramachandran, Stephane Clemmen, Roel Baets, Sean T Barry, et al. Plasma-enhanced atomic layer deposition of nanostructured gold near room temperature. *ACS applied materials & interfaces*, 11(40):37229–37238, 2019.

[71] Huan Hu, Hoe Joon Kim, and Suhas Somnath. Tip-based nanofabrication for scalable manufacturing. *Micromachines*, 8(3):90, 2017.

[72] Matthew BE Griffiths, Peter J Pallister, David J Mandia, and Seán T Barry. Atomic layer deposition of gold metal. *Chemistry of Materials*, 28(1):44–46, 2016.

[73] Nathaniel E Richey, Camila De Paula, and Stacey F Bent. Understanding chemical and physical mechanisms in atomic layer deposition. *The Journal of chemical physics*, 152(4), 2020.

[74] Joshua B Ballard, James HG Owen, Justin D Alexander, William R Owen, Ehud Fuchs, John N Randall, Roberto C Longo, and Kyeongjae Cho. Spurious dangling bond formation during atomically precise hydrogen depassivation lithography on si (100): The role of liberated hydrogen. *Journal of Vacuum Science & Technology B*, 32(2), 2014.

[75] James A Oke and Tien-Chien Jen. Atomic layer deposition and other thin film deposition techniques: from principles to film properties. *Journal of Materials Research and Technology*, 21:2481–2514, 2022.

[76] Pengfei Liu, Yuchen Zhang, Cong Liu, Jonathan D Emery, Anusheela Das, Michael J Bedzyk, Adam S Hock, and Alex BF Martinson. Thermal atomic layer deposition of gold: mechanistic insights, nucleation, and epitaxy. *ACS Applied Materials & Interfaces*, 13(7):9091–9100, 2021.